IPEM Institute of Physics and Engineering in Medicine

TOPICAL REVIEW

Magnetic resonance elastography (MRE) of the human brain: technique, findings and clinical applications

To cite this article: Lucy V Hiscox *et al* 2016 *Phys. Med. Biol.* **61** R401

View the article online for updates and enhancements.

Related content

- Multifrequency inversion in magnetic resonance elastography
  Sebastian Papazoglou, Sebastian Hirsch, Jürgen Braun et al.

- Phantom evaluations of nonlinear inversion MR elastography
  Ligin M Solamen, Matthew D McGarry, Likun Tan et al.

- Simultaneous 3D MR elastography of the in vivo mouse brain
  Steven P Kearney, Shreyan Majumdar, Thomas J Royston et al.

Recent citations

- Hippocampal viscoelasticity and episodic memory performance in healthy older adults examined with magnetic resonance elastography
  Lucy V. Hiscox *et al*

- Stiffness and Beyond
  Ziying Yin *et al*

- Group versus Phase Velocity of Shear Waves in Soft Tissues
  Kevin J. Parker *et al*

Topical Review

Magnetic resonance elastography (MRE) of the human brain: technique, findings and clinical applications

Lucy V Hiscox[1,2,8]**, Curtis L Johnson**[3]**, Eric Barnhill**[4]**,
Matt D J McGarry**[5,6]**, John Huston 3rd**[7]**,
Edwin J R van Beek**[2]**, John M Starr**[1] **and Neil Roberts**[2]

[1] Alzheimer Scotland Dementia Research Centre, University of Edinburgh, 7 George Square, Edinburgh EH8 9JZ, UK
[2] Clinical Research Imaging Centre, College of Medicine and Veterinary Medicine, University of Edinburgh, 47 Little France Crescent, Edinburgh EH16 4TJ, UK
[3] Department of Biomedical Engineering, University of Delaware, 550 S College Ave, Newark, DE 19713, USA
[4] Institute for Medical Informatics, Charité Universitätsmedizin Berlin, Germany
[5] Thayer School of Engineering, Dartmouth College, Hanover NH 03755, USA
[6] Department of Biomedical Engineering, Columbia University, New York, NY 10032, USA
[7] Department of Radiology, Mayo Clinic, 200 First Street SW, Rochester, MN 55905, USA

E-mail: l.v.hiscox@sms.ed.ac.uk

Abstract

Neurological disorders are one of the most important public health concerns in developed countries. Established brain imaging techniques such as magnetic resonance imaging (MRI) and x-ray computerised tomography (CT) have been essential in the identification and diagnosis of a wide range of disorders, although usually are insufficient in sensitivity for detecting subtle pathological alterations to the brain prior to the onset of clinical symptoms—at a time when prognosis for treatment is more favourable. The mechanical properties of biological tissue provide information related to the strength and integrity of the cellular microstructure. In recent years, mechanical properties of the brain have been visualised and measured non-invasively with magnetic resonance elastography (MRE), a particularly sensitive medical imaging technique that may increase the potential for early diagnosis. This review begins with an

[8] Author to whom any correspondence should be addressed.

introduction to the various methods used for the acquisition and analysis of MRE data. A systematic literature search is then conducted to identify studies that have specifically utilised MRE to investigate the human brain. Through the conversion of MRE-derived measurements to shear stiffness (kPa) and, where possible, the loss tangent (rad), a summary of results for global brain tissue and grey and white matter across studies is provided for healthy participants, as potential baseline values to be used in future clinical investigations. In addition, the extent to which MRE has revealed significant alterations to the brain in patients with neurological disorders is assessed and discussed in terms of known pathophysiology. The review concludes by predicting the trends for future MRE research and applications in neuroscience.

Ⓢ Online supplementary data available from stacks.iop.org/PMB/61/R401/mmedia

(Some figures may appear in colour only in the online journal)

1. Introduction

1.1. Background

Over the centuries in clinical medicine, a wide range of pathologies have been detected and characterised by manually probing soft tissue in the human body through touch. This technique, known as palpation, has been used to identify lesions through the detection of mechanical changes in tissue composition when compared to surrounding healthy tissue. As an example, clinicians differentiate between subcutaneous masses that are hard and more likely to be malignant and those that are soft and likely to be benign, such as lipomas.

Elastography describes the use of medical imaging for the quantitative measurement of soft tissue mechanical properties (Ophir *et al* 1999). A mechanical stimulus of some kind must be propagated into the tissue, as tissue mechanics cannot be measured directly. Sources to detect the resulting tissue displacements must be available, and have included ultrasound, magnetic resonance imaging (MRI) and other diagnostic imaging modalities (Parker *et al* 2011, Doyley and Parker 2014). Numerous studies have applied ultrasonic techniques to study the mechanical properties of the human brain, such as freehand quasistatic ultrasound elastography (Chakraborty *et al* 2012) and acoustic radiation force impulse imaging (ARFI) (Su *et al* 2015), with potential applications within neurosurgery and the study of the neonatal brain, respectively. Nevertheless, elastography with MRI, known as magnetic resonance elastography (MRE), has a distinct advantage over ultrasonic methods as it benefits from being both non-invasive, and capable of generating images with a high spatial resolution. As such, MRE has the potential to study a wide-range of neurological disorders, and forms the focus of this review.

MRE is a phase-contrast MRI technique that involves imaging the propagation of applied acoustic waves using a modified MRI pulse sequence (Muthupillai *et al* 1995, Muthupillai and Ehman 1996). An MRE investigation involves a conventional MRI scanner, the modified

pulse sequence incorporating motion-encoding gradients (MEG), and a source of harmonic motion to generate shear waves in to the tissue of interest. The degree of tissue displacement is determined by measuring the wavelength to ultimately infer the inherent material property. Data processing typically involves the application of a mathematical inversion algorithm that relates tissue displacement to the physics of motion, or through the use of sophisticated image processing algorithms. Displacement information can then be transformed into stiffness maps, i.e. 'elastograms'. Waves travel faster and exhibit a longer wavelength in stiffer materials. More complex models such as viscoelasticity also calculate the attenuation of the wave amplitude, providing an additional measure of tissue viscosity.

The application of MRE to the study of patients with liver disease has proven to be successful in measuring the degree of fibrosis (Loomba *et al* 2014), which presents with an increase in tissue stiffness. Importantly, MRE parameters have been corroborated with histological samples (Venkatesh *et al* 2013), biopsy-proven liver fibrosis (Asbach *et al* 2010), and displays high diagnostic accurary and inter-reader agreement (Rustogi *et al* 2012). This has resulted in MRE increasingly being used as a diagnostic tool in clinical practice as an alternative to liver biopsy, which has known complications. Other organs to have been investigated include heart (Kolipaka *et al* 2009, Elgeti *et al* 2010), breast (Sinkus *et al* 2000, 2007, Siegmann *et al* 2010) skeletal muscle (Bensamoun *et al* 2007, Chen *et al* 2008), lungs (Goss *et al* 2006, Mariappan *et al* 2014), kidney (Bensamoun *et al* 2011, Streitberger *et al* 2014a), and prostate (Arani *et al* 2013, Brock *et al* 2015), highlighting the capability for MRE to investigate a wide range of organs and associated pathologies.

The mechanical properties of soft tissue vary over a dynamic range much greater than other physical properties such as MR relaxation time—the measurement of which provides the foundation for conventional structural images (Mariappan *et al* 2010). Due to the intrinsically high dynamic range, MRE offers the prospect of an imaging technique with high sensitivity. Further, due to the difference in methodology, it would be conceivable that MRE could detect pathological changes to soft tissue occult to other forms of medical imaging.

There has recently been significant interest to investigate the mechanical properties of the human brain, especially given that direct clinical palpation is not possible outside of neurosurgery. Neurosurgeons routinely use palpation through surgical instruments to assist in identifying the brain-tumour interface. In particular, there is demand for more sensitive neuroimaging techniques to detect the early signs of neurodegeneration (i.e. preclinical Alzheimer's disease). Conventional radiological scans are used primarily to monitor the degree of atrophy—an increase of which is indicative of irreversible neuronal loss. Investigations that have combined MRE and histology with murine models of disease have suggested that inflammation (Riek *et al* 2012), toxic demyelination (Schregel *et al* 2012), and transient ischemic insult (Freimann *et al* 2013), all directly alter mechanical property measurements. These findings support the notion that mechanical imaging may be able to detect changes to the interactions and integrity of neurons, glial cells, and the vascular network *prior* to volumetric changes or neuronal loss. Identifying the prodromal stages in neurological disorders is essential in order to better understand the pathophysiological mechanisms for aiding the development of novel pharmaceutical or surgical treatment strategies.

Initial MRE studies of the brain were of several tissue slices and reported mechanical property values for global brain tissue. Subsequently, mechanical property values were quoted separately for grey and white matter. More recently, MRE has developed into a technique that can provide whole brain coverage in 3D, enabling the measurement of specific neuroanatomical regions such as the corpus callosum (Johnson *et al* 2013a), hippocampus (Johnson *et al* 2016), or corticospinal tract (Romano *et al* 2012). In addition, healthy ageing (Sack *et al* 2009,

2011), gender differences (Sack *et al* 2009, Arani *et al* 2015), and a wide range of focal and diffuse brain pathologies have been investigated.

The purpose of this review article is for introducing MRE to clinicians and medical researchers in the neurosciences, to summarise the results obtained, and review the current clinical applications being pursued.

1.2. Aims of review

This review aims to:

1. Provide a thorough description of the steps involved in performing a brain MRE investigation. This includes an introduction to the types of vibration source, a description of how cyclic motion is encoded in MRI, and how the motion encoded wave images can be processed to measure tissue mechanical properties.
2. Systematically review relevant brain MRE articles to summarise the values obtained to date for healthy participants. All MRE data will be converted to common parameters of shear stiffness (kPa), and loss tangent (rad), in order to present data on global brain tissue (GBT), grey matter (GM), and white matter (WM), including mean values, their variance and factors that may influence these values.
3. Assess the ability of MRE to reveal significant alterations in the mechanical properties of the brain in patients with neurological disorders, and how MRE findings may relate to pathophysiology.

2. MRE methodology

Put simply, the MRE technique adds to conventional MR imaging (figures 1(a) and (b)), by using motion-encoding magnetic field gradients to capture raw phase images, (figure 1(c)), that reveal the micron-level displacements produced by the propagation of applied acoustic waves (figures 1(d)–(f)). Mathematical image analysis techniques have been developed for the processing of displacement images, to produce maps of tissue stiffness i.e. elastograms (figures 1(h) and (i)). This general process, together with the alternative acquisition and analysis procedures adopted by various research groups, are described in detail below.

2.1. Induced tissue deformation

The first stage in the acquisition of MRE data is the generation of a dynamic source of motion. Potential external sources include electromagnetic (Xu *et al* 2007b, Braun *et al* 2014), acousto-mechanical (Sack *et al* 2008, Lipp *et al* 2013) pneumatic (Johnson *et al* 2014, Huston *et al* 2015), and piezoelectric (Guo *et al* 2013) devices, which transmit vibrations to the head via a passive driver such as a bite-bar, head cradle, or soft pillow. A pneumatic design is illustrated in figure 2. In this example, compressed air is transmitted from an active driver, situated in the MRI control room, to a passive soft pillow-like device placed underneath the head (Resoundant, Mayo Clinic, Rochester, MN, USA). A recent development has been the use of a soft mat placed on the thorax, coupled with a piezoeletric driver, so as to induce vibrations to the head indirectly (Fehlner *et al* 2015). Each set-up causes the head to experience a gentle nodding motion on the order of microns (typically between 5–50 μm). Alternatively, pilot studies have been performed to investigate whether brain MRE can be performed without external mechanical hardware. An MRE technique termed *intrinsic activation* has been
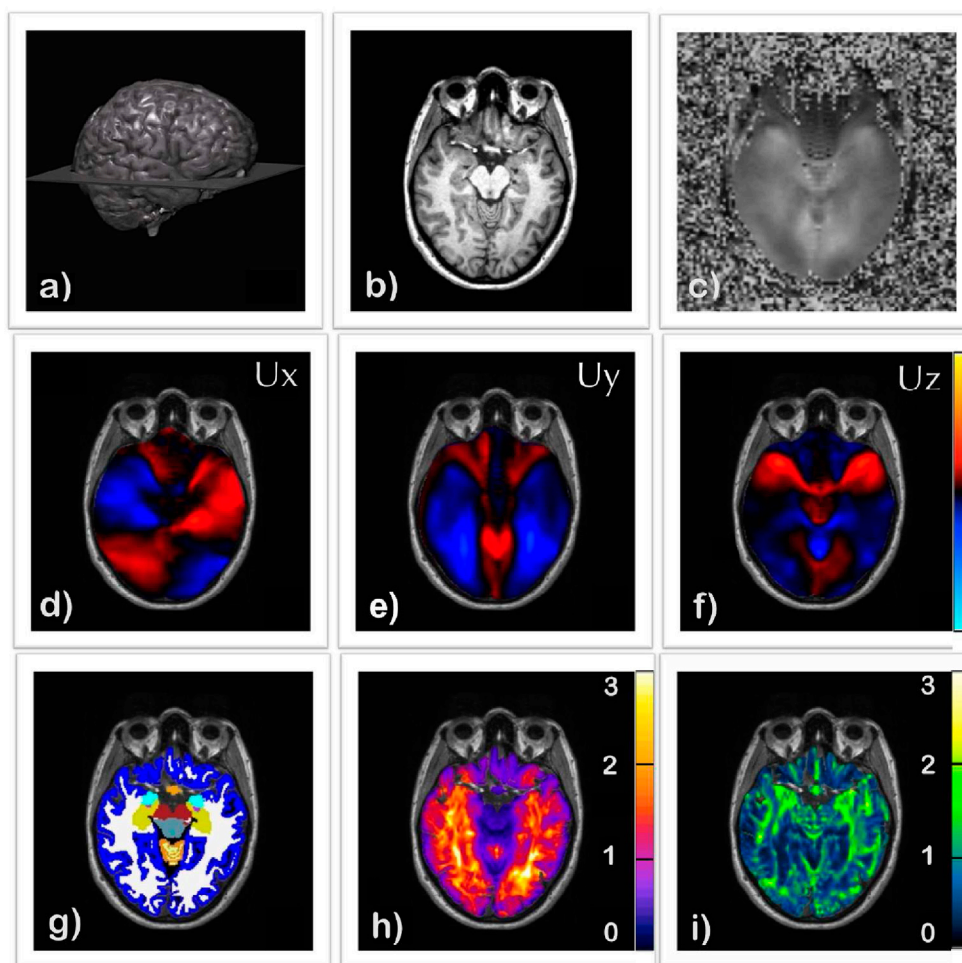
Figure 1. A typical workflow from a brain MRE investigation: (a) 3D rendering of a T1-weighted MPRAGE anatomical scan of the brain highlighting the slice of interest, (b) the aforementioned T1 axial slice, (c) raw DICOM phase image, (d)–(f) wave images from three orthogonal directions (x,y,z), indicating the degree of displacement between -5 μm and 5 μm, (g) segmented image displaying the deep brain structures in the medial temporal lobe, (h) map of the complex shear modulus magnitude $|G^*|$ (kPa) and (i) phase angle ϕ (RAD), produced via the Elastography Software Pipeline (ESP) (Barnhill *et al* 2016).

developed to measure the low frequency motion generated by the natural pulsations of the brain's blood vessels (Weaver *et al* 2012, McGarry *et al* 2015).

2.1.1. Actuation frequency. The frequency at which the brain tissue is vibrated typically ranges between 10–100 Hertz (Hz). Lower frequency waves attenuate less rapidly than higher frequency waves, enabling the analysis of deeper brain tissue. Displacements below 10 Hz, however, are generally too large and thus do not provide acceptable signal. On the other hand, high frequency waves with a shorter wavelength, can theoretically provide higher spatial resolution. Frequencies above 100 Hz are generally not used, however, due to discretisation errors (Papazoglou *et al* 2008) (i.e. where the wave cannot be sampled correctly), and for participant
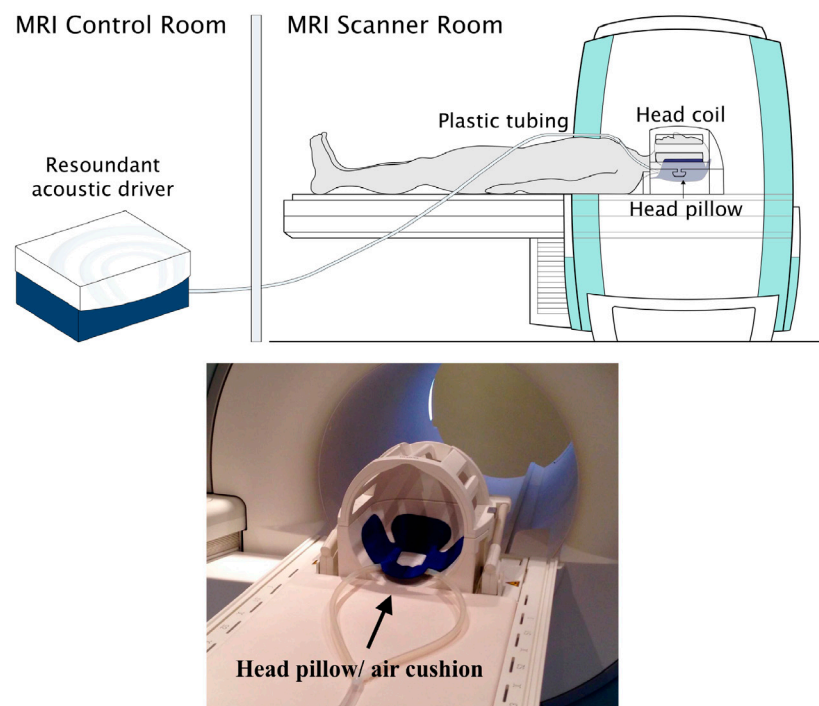
Figure 2. (a) Schematic diagram of the pneumatic actuator with head-pillow driver (Resoundant, Mayo Clinic, Rochester, MN, USA), (b) Photograph of the head-pillow within the MRI head-coil.

comfort, as higher frequencies require greater amplitude levels to penetrate the skull. A standardised frequency has not been set across different research groups, largely due to the use of alternative MRE acquisition sequences and analysis protocols. Generally speaking, the majority of brain MRE studies have used a frequency of 50 Hz–60 Hz, and requires balancing the trade-off between depth of penetration, resolving power and noise levels. Nevertheless, the amplitudes of vibration at the prescribed frequencies are well within the safety margins permitted by the European Union whole-body vibration standard—designed to limit chronic occupational exposure (Ehman *et al* 2008). In addition, within this limited frequency range (i.e. 10–100 Hz), brain mechanical properties have appeared to follow a power-law frequency dependence (Szabo and Wu 2000). Some studies have therefore utilised a range of vibration frequencies to enable rheological modelling of the frequency-dependent material properties, providing an opportunity to enhance tissue characterisation (Klatt *et al* 2007, Sack *et al* 2009). Alternatively, data from multiple frequencies have been combined to improve image resolution (Papazoglou *et al* 2012, Barnhill *et al* 2016), more details of which are provided in section 2.4.3.

2.2. Motion encoding

Conventional MRI applies a sequence of radiofrequency (RF) excitation pulses and phase and frequency encoding gradients to produce an image by encoding the spatial position of hydrogen nuclei (spins) in voxels within a tissue (Edelman and Warach 1993). For MRE, an additional cyclic *motion-encoding gradient* (MEG) is incorporated into an MRI sequence in order to spatially map and measure the displacement patterns created by the wave propagation.

In the presence of a magnetic field gradient, $\vec{G}_r(t)$, the application of the MEGs will encode the spins with trajectory, $\vec{r}(t)$, into the phase image, providing a single shot measure of the total amount of accrued phase ϕ

$$\phi(\tau) = \gamma \int_0^\tau \vec{G}_r(t) \cdot \vec{r}(t)\, dt, \tag{1}$$

where γ is the gyromagnetic ratio characteristic of the nuclear isochromat under investigation (· represents scalar product relationship between vector functions). From the phase accumulation calculated at a single time point, it is possible to infer the amount of tissue displacement at each voxel; the phase of harmonically vibrating tissue is directly proportional to its displacement.

Synchronisation of the externally applied motion with the MEG, is a critical step in the MRE acquisition process. Protons moving in synchronisation with the switching of the MEG, from one polarity to the other, will continually accumulate phase. Importantly, stationary protons, or tissue movement unrelated to the shear wave frequency will not accumulate phase, due to the balanced nature of the gradient. Manipulation of the synchrony between the MEG and the external vibration can be created by the trigger pulse, causing a small delay, known as a phase offset θ. Four or eight phase offset images are usually sampled throughout the wave cycle, in order to capture the propagating wave over the vibration period.

Accurate determination of tissue mechanical properties requires the capture of the full vector displacement field in 3D (Hamhaber *et al* 2007), with the MEG in turn imposed along all three orthogonal directions. Early MRE studies analysed two-dimensional (2D) wave propagation while assuming plane wave propagation during inversion, to enable clinical investigations to be performed in a short scan time. However, assumptions associated with 2D inversion degraded elastogram quality and the reliability of values. With advances in acquisition protocols, recent MRE studies have encoded the full 3D wave field using MEG encoding in the read-out (x), phase-encode (y) and through-plane (z) direction, either within a volumetric slab of brain tissue (Guo *et al* 2013, Lipp *et al* 2013) or throughout the entire brain (Murphy *et al* 2013b, Johnson *et al* 2014).

2.2.1. MRE pulse sequences. MEGs have been incorporated into a number of MRI imaging sequences, including gradient-recalled echo (GRE) (Xu *et al* 2007a, Kruse *et al* 2008) single-shot spin-echo echo planar imaging (EPI) (Murphy *et al* 2011, Zhang *et al* 2011, Braun *et al* 2014), multi-shot, variable density spiral (Johnson *et al* 2013b) and 3D multi-shot multi-slab spiral EPI (Johnson *et al* 2014). Producing reliable estimates of brain mechanical properties relies on MRE sequences to obtain images with adequate resolution and signal-to-noise ratio (SNR). Low resolutions do not allow regional estimates of mechanical properties, whereas noise will warrant excessive filtering, limiting the ability to detect fine scale features. The most common sequence for brain MRE has been a single-shot spin-echo EPI sequence, which is capable of acquiring 3D displacement data within a short imaging time in comparison to the original GRE sequences adapted for MRE. However, the main disadvantage is that EPI sequences are susceptible to significant distortions; the entire range of phase encoding steps are acquired in one TR (repetition time), thus leading to a long readout time. A recent development is the so-called multi-shot multi-slab spiral sequence that can capture MRE displacement data in a shorter scan time by using multiple 3D volumes, or slabs, that cover the entire brain (Johnson *et al* 2014). Due to spiral filling of k-space, read out time is reduced, leading to high SNR efficiency and less distortion from field inhomogeneities.
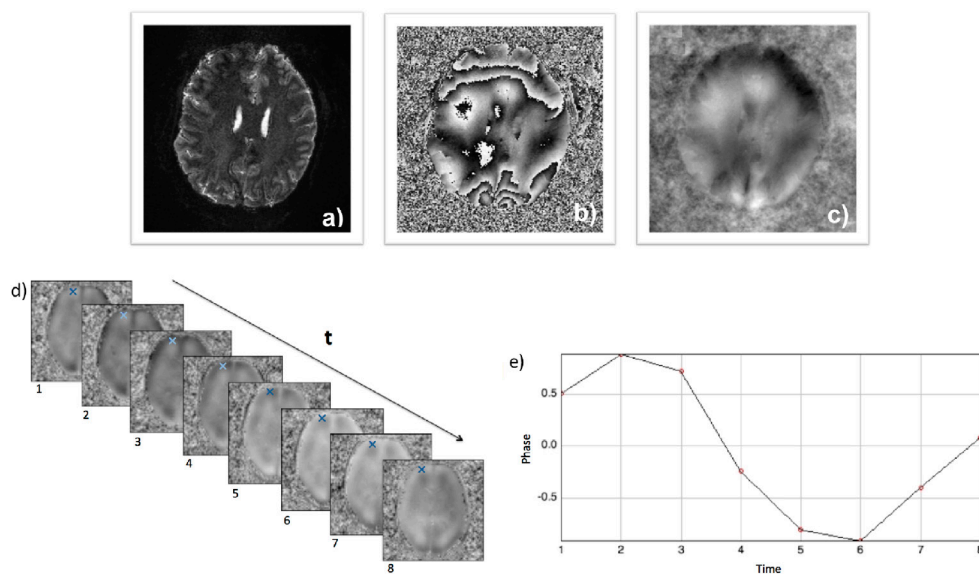
Figure 3. Phase unwrapping is a pre-requisite for all MRE phase images: (a) EPI magnitude; (b) EPI raw phase (wrapped) image; and (c) unwrapped phase image obtained using the Laplacian-based estimate (LBE) algorithm (available within PhaseTools software (Barnhill *et al* 2015)), (d) image stack of eight phase offsets for a single brain slice. Phase images have been unwrapped. The blue crosses show the voxel where the phase displacement can be visualised in the corresponding graph, (e) the change in phase over the eight time-steps, caused by the applied wave propagation.

2.3. Pre-processing of phase images

Raw phase images undergo a number of processes prior to analysis, in order to remove unwanted noise contributions. The amplitude of vibration must be sufficient to produce waves deep within the brain (Manduca *et al* 2001). However, too great an amplitude can create heavy *phase wrap*, particularly near the edges of the brain due to the phase of the wave shifting by more than 2π, see figures 3(a)–(c). Several unwrapping algorithms have been developed each with their own strengths and weaknesses relating to delivery of the exact solution, robustness to high noise, or full automation (Herráez *et al* 2002, Schofield and Zhu 2003, Barnhill *et al* 2015). Next, the phase images are temporally Fourier transformed, to obtain the frequency domain complex displacement field and to isolate the harmonic motion of interest. Removal of longitudinal waves is necessary as they may also contribute to the total measured displacement field. High-pass filtering or calculating the vector curl of the measured wave field (Sinkus *et al* 2005), are two common approaches to remove low-frequency bulk waves, and leave only the remaining high-frequency shear wave contribution. Figures 3(d) and (e) shows the sinusoidal change in phase over time after phase unwrapping and high-pass filtering.

2.4. Calculating tissue mechanical properties

A number of parameters are used to characterise the mechanical properties of materials, such as the Young's modulus (E), and bulk modulus (K). The shear mechanical properties are typically measured in MRE, and describe the strain of a material along an axis, when stressed perpendicular to that axis. Passive drivers, such as the head-pillow actuator, are utilised to induce vibrations into the targeted tissue, causing deformation and shear waves as a

result of mode conversion and complex phenomena at boundaries and interfaces. Numerous analysis techniques have been developed for calculating the shear mechanical properties including: wavelength estimation, direct inversion (DI), and non-linear inversion (NLI). Further processing has been performed by utilising the DI equation across multiple frequencies to enable rheological modelling or multi-parameter elasto-visco inversion (MDEV), as described below.

2.4.1. Wavelength estimation. The earliest approach for analysing MRE data was the measurement of the wavelength and represents a simple and intuitive approach to identify the elastic shear modulus G. The shear wave speed (ν_s) is a function of the applied mechanical frequency (f) and the wavelength (λ), and is related to an approximated density ρ ($\sim 1000\,\mathrm{kg\,m^{-3}}$) (Burlew *et al* 1980), and elastic shear modulus G by the following relationship:

$$G = \rho\nu_s^2 = \rho(\lambda f)^2 \tag{2}$$

Manual measurements of the wavelength were initially made using calipers (Bensamoun *et al* 2006), before the subsequent development of an automatic algorithm known as the local frequency estimation (LFE) (Knutsson *et al* 1994, Manduca *et al* 1996). The LFE algorithm uses a series of multiscale filters in order to estimate the spatial frequency (f_{sp}), thereby applying an image processing approach to MRE analysis: $G = f^2/f_{sp}^2$. Wavelength estimates can, however, be corrupted by the effect of dilatational waves, rigid body motion and boundary reflections, limiting the validity of both the caliper and LFE methods.

More recently, both the elastic and viscous (i.e. viscoelastic) tissue properties have been determined by calculating the *complex* shear modulus G^*, where the complex quantity G^* can be decomposed into real and imaginary components:

$$G^* = G' + iG'', \tag{3}$$

with G' the real part of the shear modulus being a measure of the mechanical energy stored in the system, and the imaginary component G'' providing a measure of the energy dissipated. The energy lost in the material is represented by the wave attenuation; a greater loss in wave amplitude indicating greater material viscosity (Guo *et al* 2012, Posnansky *et al* 2012). Note that for purely elastic materials, there is no phase lag or dissipation, as expected, and the imaginary component will be zero.

Alternatively, the magnitude $|G^*|$ and phase angle ϕ of the complex modulus, or loss tangent, can be reported, where $|G^*| = \sqrt{G'^2 + G''^2}$ and $\phi = \arctan(G''/G')$, respectively. The magnitude of the tissue response is the parameter most similar to the information afforded by manual palpation (Sack *et al* 2013), as the total response includes both the displacement (elasticity) and rate of displacement (viscosity). The phase angle ϕ is a common measure of relative tissue viscosity, with a higher value indicating greater dissipative behaviour and a more complex tissue network structure (Riek *et al* 2012). The phase angle ϕ is usually reported as a measure of tissue viscosity due to the loss moduli being an order of magnitude smaller than the storage moduli, and therefore susceptible to error and lower relative sensitivity. For a summary of MRE parameters, see table 1.

In a visocelastic material, the shear wavespeed is affected by both elastic and viscous properties, through the equation (Manduca *et al* 2001):

$$G_s = \rho\nu_s^2 = \frac{2(G'^2 + G''^2)}{G' + \sqrt{(G'^2 + G''^2)}}. \tag{4}$$

Table 1. Summary of MRE parameters.

MRE parameter	Description
Wavelength parameters	
Elastic shear modulus G	Measure of tissue stiffness in an elastic material obtained by directly measuring wavelength. Defined as the product of wave speed squared times density. Units of **kPa**
Shear stiffness G_s	Determines the wavelength in a viscoelastic material. Necessary to compute the complex shear modulus prior to the shear stiffness calculation, see equation (4). Units of **kPa**
Complex shear modulus	
Storage modulus G'	Real component of the complex shear modulus and a measure of the restoration of mechanical energy due to the elastic properties of the material. Related to the inherent mechanical rigidity of the tissue matrix. Units of **kPa**
Loss modulus G''	Imaginary component of the complex shear modulus and a measure of the energy dissipated in tissue as a result of the mechanical friction inherent to the material. In some cases is used as a viscosity parameter. Units of **kPa**
Magnitude $|G^*|$	Magnitude of the complex shear modulus and a measure of the total response of tissue to harmonic vibration. Includes both elastic and viscous information and thus may relate to haptic distinction between stiff and soft materials. Units of **kPa**
Phase angle ϕ (loss tangent)	Phase angle of the complex shear modulus is used to describe the dissipative behaviour of tissue determined by the cellular network. The higher the ratio, the more viscous and complex the tissue structure. ϕ is determined from $\arctan G''/G'$. Units of **radians**
Modelling parameters	
Spring pot parameter μ	Parameter of the spring-pot model reflecting both elastic and viscous frequency-independent information. Related to the solid-fluid behaviour of tissue, which in turn reflects cellular strength and connectivity. Units of **kPa**
Spring pot powerlaw exponent α	Parameter of the spring-pot model reflecting brain tissue geometry or structure. Has been found to correlate with the fractal dimension (complexity) of the tissue network and corresponds to the alignment of structural building blocks. A **dimensionless** quantity

In this case, the wavespeed is the undamped shear modulus, and is typically known as the shear stiffness G_s. i.e. the effective stiffness at the actuation frequency. In order to calculate the shear stiffness, it is necessary to obtain the complex shear measurements via the direct inversion algorithm, see section 2.4.2.

2.4.2. Single frequency direct inversion (DI). An advance in MRE processing involves calculating tissue mechanical properties through the equations of motion that describe wave propagation within a medium (Oliphant *et al* 2001). Direct inversion (DI) involves directly inserting the measured displacements into the appropriate wave equation governing the material, and importantly, can include viscous, anisotropic and geometric effects. The inversion problem is complex and a number of assumptions are required in order to reach a solution; assumptions are often employed to create a simple mathematical model of a tissue system. The constitutive equation of motion for a homogeneous, linear, anisotropic, viscoelastic material relates an applied stress to the resulting strain through the expression of a rank 4 tensor with 21 independent complex quantities (Mariappan *et al* 2010). Making the assumption of isotropy

(i.e. tissue does not exhibit direction-dependant properties), reduces the number of independent quantities to two: the Lamé constants λ and G. G is the proportionality constant between shear stress and shear strain and is known as the shear modulus, and λ is a parameter related to the compressibility of the material, $\lambda \to \infty$ as a material approaches the incompressible limit. With these assumptions, the equation for harmonic motion is:

$$G^*\nabla^2\boldsymbol{u}(f) + (\lambda + G^*)\nabla(\nabla \cdot \boldsymbol{u}(f) = -\rho\omega^2\boldsymbol{u}(f) \tag{5}$$

where $\boldsymbol{u}$ is the vector displacement field, ρ tissue density ($\sim 1000\,\text{kg m}^{-3}$), ∇^2 the Laplace operator, and ω the angular frequency, $\omega = 2\pi f$, where f is the applied mechanical frequency (Hz). The first Lamé parameter λ is approximately six orders of magnitude greater than G, making the simultaneous calculation of both parameters impractical and unnecessary—which warrant the removal of λ, as previously discussed in section 2.3. Consequently, equation (5) can be simplified to the Helmholtz equation by assuming tissue incompressibility ($\nabla \cdot \boldsymbol{u}(f) = 0$)—a reasonable assumption for the brain due to the large water content

$$G^*\nabla^2\boldsymbol{u}(f) = -\rho\omega^2\boldsymbol{u}(f). \tag{6}$$

This equation directly relates the measured displacements to the complex shear modulus G^* by the angular frequency ω and the material density ρ.

The greatest practical limitation of single-frequency DI is the use of the Laplacian (2nd order derivatives), resulting in high noise sensitivity. In addition, single frequency DI is susceptible to wave nodes, (regions without deformation), resulting in the inability to recover elastographic signal. More generally, DI techniques assume tissue mechanical properties are locally constant in order to simplify the equation (the so-called homogeneity approximation), despite the brain being a heterogeneous structure with different constituents likely to possess diverse non-linear, viscoelastic, and anisotropic mechanical properties. Attempts have been made to take first order spatial derivatives into account in order to overcome this assumption although this approach has yet to be applied to the brain (Sinkus *et al* 2010). Other studies have corrected for the isotropic assumption during the inversion procedure after the determination of nerve fibre orientation supplied from diffusion-tensor imaging (DTI) (Romano *et al* 2012, 2014).

2.4.3. Non-linear inversion using finite-element models (NLI). Finite element modelling (FEM) is a numerical method of achieving approximate solutions to problems in solid mechanics using partial differential equations. FEM methods are known as the "forward problem", as prior knowledge of tissue geometry, boundary conditions, and mechanical properties are needed to initially build a model simulation (Van Houten *et al* 1999, McGarry *et al* 2012). Elastograms are generated by iteratively updating a heterogeneous property distribution in a model of the tissue to minimise the difference between experimentally measured and theoretically predicted data. An initially complex system is subdivided into a collection of small overlapping subzones to reduce the computational cost. Once these subzones have been estimated, an approximation of the overall system can be obtained from the union of all subzone solutions. The process is complete once the calculated displacements predicted by solution of the forward problem agree suitably with the measured displacements. FEM-based approaches have the advantage of being able to incorporate the full equations of motion, and mechanical models such as Rayleigh damping (McGarry and Van Houten 2008, Van Houten *et al* 2011, Van Houten 2014) or poroelasticity (Perrinez *et al* 2010, McGarry *et al* 2015), which go beyond the assumptions of linear elasticity and viscoelasticity. The major limitation with NLI is the speed of processing, which is on the order of hours. In contrast, DI can be performed within seconds and thus more suited to fit within a clinical radiological workflow.

2.4.4. Additional processing—multi-frequency MRE.

Rheological modelling. Mechanical properties derived from single wave frequency studies are a function of frequency, and therefore bound to specific experimental conditions. An alternative analysis technique has utilised the DI equation over multiple vibration frequencies in order to acquire the dispersion function of the complex shear modulus in order to improve the physical significance of MRE data (Klatt *et al* 2007, Sack *et al* 2009). Multifrequency acquisitions have been acquired at, for example, 25, 37.5, 50 and 62.5 Hz, and the dispersion of waves across this frequency range are analysed for the ability to fit a prescribed rheological viscoelastic model. Viscoelastic models include the Maxwell model, Kelvin-Voigt model, and the Zener model, among others (Schiessel *et al* 1995, Asbach *et al* 2008). The spring-dashpot parameter model has been determined to be the most suitable viscoelastic model for biological tissue, in which tissue is characterised by an hierarchical arrangement of elastic springs μ and viscous dashpots η (Sack *et al* 2009). While linear models do not show a power-law frequency dependence, shear moduli data can be fitted to a fractional spring-dashpot model:

$$G^* = \kappa(i \cdot 2\pi \cdot f)^\alpha \qquad\qquad (7)$$

with $\kappa = \mu^{(1-\alpha)}\eta^\alpha$ yielding frequency independent elasticity μ, frequency independent viscosity η and a tissue characterisation constant α. As μ and η are co-dependent, η is assumed constant and assigned a value of 3.7 Pa—previously calculated as an approximate value of viscosity in human brain tissue (Klatt *et al* 2007). Ultimately, two frequency-independent material parameters are reported. μ combines elasticity (stiffness) and viscosity (friction) in one parameter to describe the solid-fluid behaviour of the tissue, and is thus a measure of adhesion and soft tissue connectivity. The slope of the modulus dispersion is analysed to provide parameter α, which characterises the alignment of mechanical structure-building elements in the tissue. α is known as the *geometry* parameter due its correlation with the fractal dimension, indicating the sensitivity of α to material complexity (Guo *et al* 2012). As a side note, α is not comparable to the loss tangent ϕ, which in general is frequency dependent. However, in some complex and irregular materials, ϕ becomes less sensitive to frequency and thus $\phi = \alpha \times \pi/2$, may hold true (Urayama *et al* 2009).

Multi-frequency dual parameter elasto-visco inversion (MDEV). Another alternative and innovative MRE analysis approach is to utilise the Helmholtz equation over several actuation frequencies and include a summation within a single inversion using an algebraic least-squares solution related to the spring-pot model (Papazoglou *et al* 2012). In contrast to the above-mentioned modelling studies, MDEV assumes, for convenience, that tissue does not exhibit frequency dependence over a small range of frequencies. Benefits of this approach include compensation for amplitude nulls and noise by averaging the magnitude displacements in each voxel, providing better-conditioned wave patterns for inversion (Fehlner *et al* 2016). MDEV reveals details of brain anatomy in a pixel-wise resolution (Guo *et al* 2013, Braun *et al* 2014), that clearly outperforms the resolution of single-frequency DI (Sack *et al* 2011). MDEV, like single-frequency based DI, however, assumes local homogeneity, and thus the quantitative performance in heterogeneous tissue is expected to be limited. Further, since the parameters provided by MDEV are

based on measurements obtained at multiple frequencies and combined to two purportedly frequency-independent parameters, $|G^*|$ and ϕ, values are not directly comparable to those predicted by single-frequency based MRE.

2.5. Standardising results across the literature

Within and across MRE research groups, numerous parameters are used to describe the mechanical properties of the brain. In order to provide a summary of results, it is necessary to standardise results according to a similar parameter, which will represent the same underlying mechanical response. Shear stiffness describes the resistance of a material to a harmonic shear stress at the given actuation frequency, and is related to the wavespeed in a viscoelastic material with density of $1000\,\mathrm{kg\,m^{-3}}$ (Manduca *et al* 2001, Johnson *et al* 2016). The relationship between shear stiffness and the complex shear modulus, is defined in equation (4), and allows for the mathematical conversion between the two parameters. For studies that have reported modelling parameters μ and α, shear stiffness can be calculated from the complex shear modulus data obtained at any frequency (for the purpose of this review, we will choose 50 Hz). We have chosen to convert values to the shear stiffness, as opposed to the magnitude of the complex modulus $|G^*|$, as this affords us with the most data to summarise and review. Studies that report the shear stiffness do not usually report values for the storage and loss modulus, rendering it impossible to calculate $|G^*|$. In addition, the shear stiffness describes the effective *stiffness* in a viscoelastic material, and is thus comparable to data that report the elastic shear modulus G. Ultimately, the shear stiffness and elastic shear modulus can collectively be referred to as 'stiffness', and is a concept more readily understood. Where possible, the loss tangent will also be calculated which is equal to $\arctan(G''/G')$, with a great angle indicating more dissipative (i.e. viscous) behaviour. These equations will later form a key part of this review, enabling the standardisation of results obtained across the literature. After searching for the relevant literature, we will use this concept to standardise results obtained for global brain tissue, grey and white matter.

3. Searching the literature

Relevant publications were found by searching three electronic databases. Inclusion and exclusion criteria were applied to identify studies with insufficient relevance to the review question before full texts were read and labelled. Our full strategy for identifying relevant literature can be found in appendix 1 of the supplementary material (available at: stacks.iop. org/PMB/61/R401/mmedia).

3.1. Studies identified

Forty-one studies referring to MRE investigations performed in a total of 914 subjects met the inclusion criteria. The corresponding authors represented MRE research groups in four different countries: USA, Germany, Australia, and China. All studies that have been identified in this review are listed in table 2. Twenty-four studies utilised MRE in the study of healthy participants, and seventeen studies investigated neurological disorders in patient populations. Ten of the seventeen clinical studies included a control group of healthy participants.

Table 2. The 41 studies identified which have investigated the mechanical properties of the human brain using MRE.

Author	Brain structure	Population	N	Age range
Klatt *et al* (2007)	GBT	Controls	5	25–46
Sack *et al* (2008)	GBT	Controls	6	34.5[a]
Sack *et al* (2009)	GBT	Controls	55	18–88
Weaver *et al* (2012)	GBT	Controls	6	22–55
Hatt *et al* (2015)	GBT	Controls	9	32.6[a]
Dittmann *et al* (2015)	GBT	Controls	8	25–54
Sack *et al* (2011)	GBT & inner, cortical, frontal, dorsal regions	Controls	66	18–72
Murphy *et al* (2013b)	GBT & frontal, occipital, parietal, temporal lobes, cerebellum, deep GM/WM	Controls	10	23–55
Arani *et al* (2015)	GBT & frontal, occipital, parietal, temporal lobes, cerebellum, deep GM/WM	Controls	45	56–89
McCracken *et al* (2005)	GM & WM	Controls	6	n/a
Xu *et al* (2007b)	GM & WM	Controls	3	28–32
Green *et al* (2008)	GM & WM	Controls	5	23–61
Kruse *et al* (2008)	GM & WM	Controls	25	23–79
Clayton *et al* (2012)	GM & WM	Controls	6	19–42
Johnson *et al* (2013b)	GM & WM	Controls	3	24–52
Braun *et al* (2014)	GM & WM	Controls	5	26–55
Zhang *et al* (2011)	GM & WM & cerebellum	Controls	8	22–43
Johnson *et al* (2013a)	GM & WM, corpus callosum, corona radiata	Controls	6	24–52
Johnson *et al* (2014)	GM & WM, brain stem, cerebellum	Controls	3	26–38
Romano *et al* (2012)	Corticospinal tract	Controls	5	25–50
Guo *et al* (2013)	WM, thalamus, corpus callosum genu, caudate nucleus	Controls	23	22–72
Fehlner *et al* (2015)	Crus cerebri, capsula interna, pons	Controls	12	27–54
Johnson *et al* (2016)	Amygdala, hippocampus, putamen, caudate, pallidum, thalamus	Controls	28	18–33
Schwarb *et al* (2016)	Hippocampus, parahippocampal gyrus, entorhinal cortex	Controls	20	18–33

Author	Disorder	Brain structure	Population	N	Age range
Xu *et al* (2007a)	Intracranial tumours (various)	GBT	Patients	6	16–63
Murphy *et al* (2013a)	Meningioma	TR	Patients	12	n/a
Simon *et al* (2013)	Intracranical tumours (various)	TR, HRT	Patients	16	26–78
Reiss-Zimmermann *et al* (2014)	Intracranical tumours (various)	TR, HRT	Patients	27	36–86
Streitberger *et al* (2014b)	Glioblastoma Multiforme	TR, HRT	Patients	22	64.5[a]
Hughes *et al* (2015)	Meningioma	TR	Patients	14	59[a]
Wuerfel *et al* (2010)	Multiple sclerosis (relapse-remitting)	GBT	Patients	45	21–51
			Controls	34	18–59

(*Continued*)

Table 2. (*Continued*)

Author	Disorder	Brain structure	Population	N	Age range
Murphy *et al* (2011)	Alzheimer's disease	GBT	Patients	7	76–94
			Controls	14	75–89
Streitberger *et al* (2010)	Normal pressure hydrocephalus	GBT	Patients	20	69.1[a]
			Controls	25	62.1[a]
Freimann *et al* (2012)	Normal pressure hydrocephalus (pre/post shunt)	GBT	Patients	20	51–85
Streitberger *et al* (2012)	Multiple sclerosis (chronic-progressive)	GBT	Patients	23	51.5[a]
			Controls	38	48[a]
Lipp *et al* (2013)	Parkinson's disease & progressive Supra-nuclear palsy	GBT, basal ganglia	PD patients	18	63[a]
			PSP patients	16	70[a]
			Controls	18	64[a]
Romano *et al* (2014)	Amyotropic lateral sclerosis	Corticospinal tract	Patients	14	46–70
			Controls	14	45–69
Huston *et al* (2015)	Fronto-temporal dementia	GBT, frontal, occipital, parietal	Patients	5	53–65
		temporal lobes, cerebellum, deep GM/WM, sensory/motor strip	Controls	9	55–66
Fattahi *et al* (2015)	Normal pressure hydrocephalus	GBT, frontal, occipital, parietal	Patients	10	67–79
		temporal lobes, cerebellum, deep GM/WM	Controls	21	67–80
Fehlner *et al* (2016)	Clinically isolated syndrome	GBT, WM	Patients	17	22–47
			Controls	33	18–53
Murphy *et al* (2016)	Alzheimer's disease & Mild cognitive impairment (MCI)	GBT, frontal, occipital, parietal temporal lobes, cerebellum, deep GM/WM, sensory/motor, FPT	AD patients	8	n/a
			MCI patients	8	n/a
			CN + controls	16	n/a
			CN—controls	16	n/a

GBT = global brain tissue, WM = white matter, GM = grey matter, TR = tumour region, HRT = healthy reference tissue. [a]Mean age of subjects.

4. Results of MRE studies of the brain in healthy subjects

This section of the review focuses on the results obtained from MRE studies of the human brain in healthy participants. We will report brain mechanical properties using common parameters of shear stiffness and loss tangent, representing tissue stiffness and relative viscosity, respectively, to standardise results among different research groups. We will first review studies that have reported the mechanical properties of the brain as a whole, henceforth referred to as global brain tissue (GBT). Second, we will report the findings from studies that have measured both grey matter (GM) and white matter (WM) as separate compartments. Finally, we will review the results from studies to have provided stiffness measurements for a range of neuroanatomical regions.

4.1. MRE results for global brain tissue (GBT)

MRE values for GBT in healthy subjects have been reported in 13 studies, and converted to shear stiffness (kPa) and loss tangent (rad), where possible, see table 3. Published values can be found in table 1 of appendix 2 in the supplementary material (available at stacks.iop.org/PMB/61/R401/mmedia). Values for the shear stiffness range between 0.62 kPa–2.99 kPa, see figure 4(a), and loss tangent varies between 0.09 rad–0.70 rad, see figure 4(b). For the 5 studies conducted using a actuation frequency of 50 Hz, mean shear stiffness and loss tangent is 2.07 kPa ± 0.42 kPa and 0.41 rad ± 0.06 rad, respectively, representing data from 198 participants.

To investigate the effect of frequency on shear stiffness, the mean values from all studies was averaged at each frequency, and calculated from spring-pot studies at all four frequencies (25, 37.5, 50 and 62.5 Hz). A simple linear regression analysis was performed to determine the relationship between shear stiffness and actuation frequency for GBT in healthy participants.

Table 3. MRE results for GBT in healthy participants.

Author	N	Inversion	f in Hz	Shear stiffness (kPa)	Loss tangent (rad)
Dittmann *et al* (2015)	8	MDEV	10, 15, 20	0.62 ± 0.08	0.09 ± 0.17
			10, 20, 30, 40, 50	1.38 ± 0.20	0.24 ± 0.10
Fehlner *et al* (2016)	33	MDEV	30, 35, 40, 45, 50, 55, 60	1.62 ± 0.18	0.61 ± 0.04
Hatt *et al* (2015)	9	DI	30	1.03 ± 0.09	0.70 ± 0.21
Sack *et al* (2009)	55	MF-SP	50	1.69 ± 0.26	0.38 ± 0.06
Wuerfel *et al* (2010)[a]	34	MF-SP	50	1.82 ± 0.22	0.38 ± 0.08
Streitberger *et al* (2010)[a]	25	MF-SP	50	2.30 ± 0.30	0.47 ± 0.12
Sack *et al* (2011)	66	MF-SP	50	2.52 ± 0.32	0.47 ± 0.07
Lipp *et al* (2013)[a]	18	DI	50	2.05 ± 0.19	0.26 ± 0.04
Murphy *et al* (2013b)	10	DI	60	2.99 ± 0.02	n/a
Arani *et al* (2015)	45	DI	60	2.59 ± 0.10	n/a
Huston *et al* (2015)[a]	9	DI	60	2.76 ± 0.08	n/a
Fattahi *et al* (2015)[a]	21	DI	60	2.55 ± 0.11	n/a
Murphy *et al* (2016)[a]	32	DI	60	2.51 ± 0.09	n/a

Note. Values show mean ± standard deviation (SD).
[a] Control data from clinical studies. n/a = not available.
Published values can be found in table 1 of appendix 2 in the supplementary material.
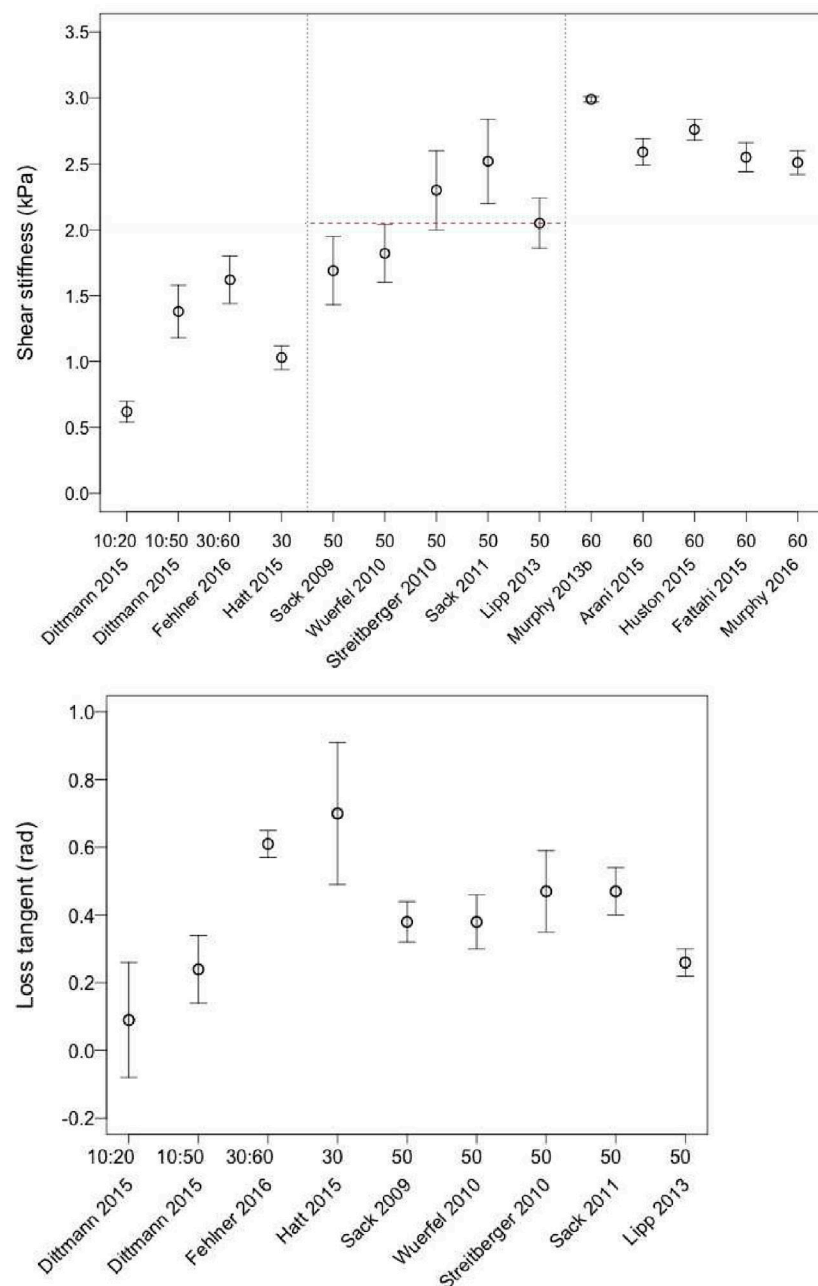
Figure 4. (a) Shear stiffness (kPa) and (b) loss tangent (rad) of global brain tissue (GBT) in healthy participants. Values show mean and standard deviation (SD). First *x*-axis displays the actuation frequency *f*, secondary axis displays study reference

A significant regression equation was found $F(1,4) = 15.31$, $p = 0.02$, with an R^2 of 0.793. Participants' predicted shear stiffness is equal to $0.443 + 0.035$ (frequency) (kPa) when frequency is measured in Hz, equating to an increase in brain stiffness of 0.4 kPa for each 10 Hz increase in frequency.

Table 4. MRE studies investigating grey matter (GM) and white matter (WM) in healthy participants.

				GM		WM	
Author	N	Approach	f in Hz	Shear stiffness (kPa)	Loss tangent (rad)	Shear stiffness (kPa)	Loss tangent (rad)
Braun *et al* (2014)	5	MDEV	30, 40, 50, 60	0.98 ± 0.25	0.95 ± 0.03	1.16 ± 0.29	1.03 ± 0.04
Johnson *et al* (2013a)	3	NLI	50	2.01 ± 0.08	0.37 ± 0.18	2.86 ± 0.13	0.46 ± 0.15
Johnson *et al* (2013b)	7	NLI	50	2.41 ± 0.19	0.48 ± 0.17	3.30 ± 0.35	0.52 ± 0.20
Clayton *et al* (2012)	5	LFE	60	3.77 ± 0.50	0.50 ± 0.27	4.16 ± 0.17	0.54 ± 0.08
McCracken *et al* (2005)	6	DI	80	5.30 ± 1.30	n/a	10.70 ± 1.40	n/a
Zhang *et al* (2011)	8	DI	80	2.72 ± 0.22	0.44 ± 0.14	2.85 ± 0.36	0.47 ± 0.28
Green *et al* (2008)	5	DI	90	4.48 ± 0.31	0.68 ± 0.10	4.24 ± 0.31	0.75 ± 0.10
Kruse *et al* (2008)	25	LFE	100	5.22 ± 1.15	n/a	13.60 ± 3.19	n/a

Note. Values show mean $\pm$ standard deviation (SD). n/a = not available.
Published values for each study can be found in table 2 of appendix 2 in the supplementary material.

4.2. Grey and white matter results

A total of 10 studies have reported the mechanical properties of both GM and WM. Published values can be found in appendix 2 (table 2; available at stacks.iop.org/PMB/61/R401/mmedia). We will report quantitative data from 8 of the 10 studies, see table 4. Exclusion for two studies is due to one study providing a qualitative analysis of wave propagation (Xu *et al* 2007b), whereas data from only 1 subject is provided in the other (Johnson *et al* 2014).

Nine out of the 10 studies reported WM to be stiffer than GM, with 6 of these studies finding a statistically significant difference. One study reported that GM was stiffer than WM (Green *et al* 2008). Shear stiffness values for GM range between GM 1.13 kPa–5.30 kPa, and for WM 1.43 kPa–13.60 kPa, see figure 5(a). WM was found to be more viscous than GM in all studies, as demonstrated by the loss tangent, see figure 5(b). The loss tangent for GM range between 0.37 rad–0.95 rad, and 0.47 rad–1.03 rad for WM.

4.3. Towards a measure of regional neuroanatomy

The mechanical properties of various brain regions have been investigated in a number of recent studies (Guo *et al* 2013, Johnson *et al* 2013a, 2016, Murphy *et al* 2013b, Arani *et al* 2015, Huston *et al* 2015). In studies characterising lobes of the brain, all were in agreement that the stiffest region of the brain was the deep GM/WM—categorised by the authors as a composite region containing structures such as the thalamus, hypothalamus, and subthalamus (Murphy *et al* 2013b, 2016, Arani *et al* 2015, Huston *et al* 2015), see table 5 and figure 6. This agrees with findings by Johnson *et al* that showed deep WM tracts (Johnson *et al* 2013a), and subcortical GM structures (Johnson *et al* 2016) were stiffer than general cerebral tissue. In contrast, the cerebellum was found to be the softest region investigated, supporting findings from Zhang *et al* (2011) who found both GM and WM of the cerebellum to be softer than the corresponding compartments of the cerebrum.

Mechanical properties of a number of neuroanatomical structures have been measured, a full summary of which goes beyond the scope of this review. Using multifrequency MRE and MDEV inversion, Guo *et al* (2013) found decreasing $|G^*|$ values in the order of WM, corpus callosum genu, thalamus, and the head of the caudate nucleus. Johnson *et al* (2013a) used their multi-shot multi slab sequence with non-linear FEM, and found WM to be softer, as determined by G', than either the corpus callosum or the corona radiata, whereas the corpus
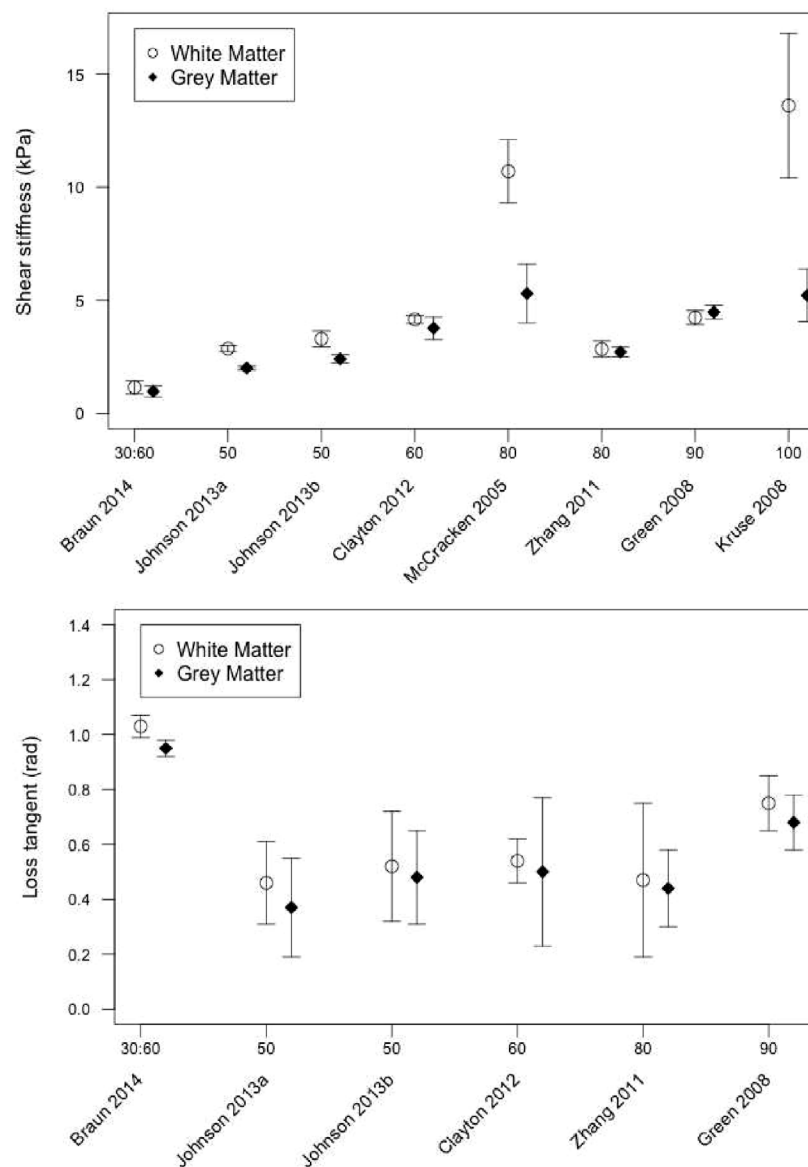
Figure 5. (a) Shear stiffness (kPa), and (b) loss tangent (rad), of GM and WM in healthy participants, showing mean ± standard deviation (SD). First *x*-axis displays the actuation frequency *f*, secondary axis displays study reference.

callosum exhibited a higher stiffness and lower viscous damping, represented by G'', compared to the corona radiata. Using waveguide elastography, the corticospinal tract (CST) was found to be approximately twice as stiff as WM (Romano *et al* 2012). The development of a new remote driver was tested by Fehlner *et al* (2015), using MDEV between the frequency range 25–45 Hz. An increase in $|G^*|$ was revealed within the CST in the the cranial-caudal direction from the capsula interna (CI) to the crus cerebri (CC), whereas the pons was softer than both the CI and CC. The fibres in the superior region of the CST (CC) showed greater

Table 5. MRE studies investigating brain regions in healthy participants.

Study author	Murphy *et al* (2013b)	Huston *et al* (2015)	Arani *et al* (2015)	Murphy *et al* (2016)
N	10	9	45	32
Mean age	23–55	61	74	n/a
Frontal lobe	3.15 ± 0.04	2.95 ± 0.10	2.70 ± 0.02	2.65 ± 0.15
Temporal lobe	3.17 ± 0.04	3.00 ± 0.13	2.80 ± 0.02	2.69 ± 0.11
Occipital lobe	3.21 ± 0.04	2.92 ± 0.09	2.80 ± 0.03	2.65 ± 0.13
Parietal lobe	2.87 ± 0.03	2.70 ± 0.08	2.60 ± 0.02	2.42 ± 0.10
Deep GM/WM	3.41 ± 0.07	3.12 ± 0.33	3.00 ± 0.02	2.79 ± 0.25
Cerebellum	2.38 ± 0.03	2.36 ± 0.16	2.20 ± 0.02	2.15 ± 0.11
Sensory-motor	n/a	2.99 ± 0.18	2.80 ± 0.03	2.82 ± 0.29

Note. Values show mean shear stiffness (kPa) ± standard deviation (SD). n/a = not available.
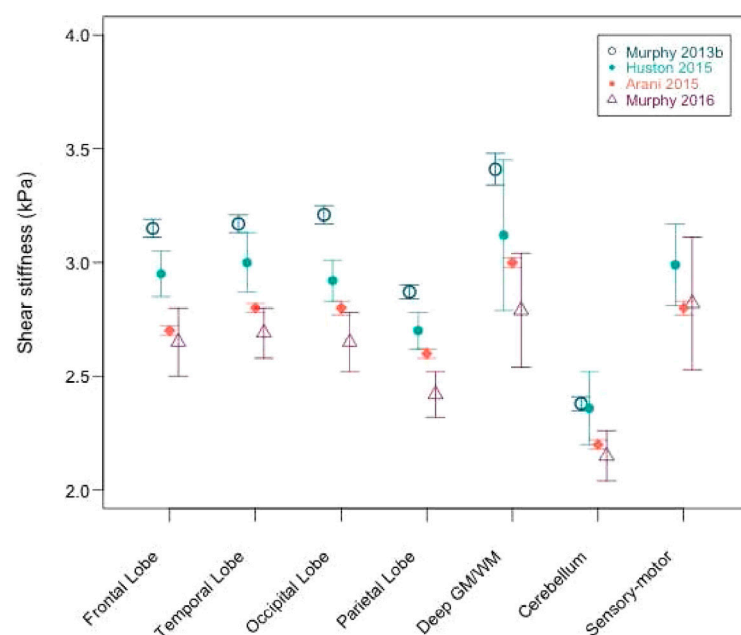
Figure 6. Regional shear stiffness (kPa) values in healthy participants.

dissipative behaviour, as determined by ϕ, followed by the CI and pons, respectively. Johnson *et al* (2014) reported higher values for the storage modulus G' within the brainstem, compared to cerebral or cerebellar tissue. Finally, Johnson *et al* (2016) found the putamen to be the stiffest and out of seven subcortical GM structures investigated, whereas the hippocampus was the softest—albeit still stiffer than general brain tissue.

5. MRE results from clinical studies

MRE has been used to investigate brain mechanical properties in a wide range of neurological disorders. These include focal intracranial tumours (ICT), as well as diffuse diseases such as Alzheimer's disease (AD) and multiple sclerosis (MS). In the previous section, output

parameters for GBT, GM and WM were converted, where possible, to measures of shear stiffness and loss tangent ϕ. In the following review of findings from clinical studies, the original MRE parameters will be maintained in order to report consistent changes according to the published findings. Although not directly comparable, shear stiffness, $|G^*|$ and μ are all similar in meaning, referring to stiffness or cellular strength, whereas both ϕ and α relate to the dissipative behaviour of tissue, or complexity of the tissue network.

5.1. Focal diseases

MRE has been used as an investigative tool to study the mechanical properties of various intracranial tumours that span the full spectrum of gradings determined by the World Health Organization (WHO), such as meningioma and glioblastoma multiforme (GBM). MRE investigations into brain tumours can be generally grouped into two categories, (i) studies of the concordance between MRE results and *in vivo* surgical manual palpation, or (ii) studies of the sensitivity or specificity of MRE for the differential diagnosis of intracranial tumours.

5.1.1. (i) Concordance between MRE results and manual palpation. Knowledge of the consistency of brain tumours prior to surgical resection, could assist surgeons in preoperative planning, improving both patient care and work-flow optimisation. Differentiation of brain tumours from healthy tissue, during surgical resection is, for the most part, based on their differing mechanical properties. Dissection of stiff, fibrous tumours are typically more difficult and present an increased risk to the patient, whereas soft tumours are usually more easily removed with minimally invasive procedures (Murphy *et al* 2013a). Three studies have obtained MRE measurements in patients prior to surgery, and have subsequently compared results with the surgeon's manual assessment, in order to assess the ability of MRE to accurately predict tumour stiffness, and hence procedural difficulty (Xu *et al* 2007a, Murphy *et al* 2013a, Hughes *et al* 2015).

The relationship between MRE results and brain palpation was first assessed by Xu *et al* (2007a) in 6 patients with diverse tumour classifications. A visual inspection of the wave propagation was correlated with the intraoperative assessment of tumour consistency determined by the neurosurgeon during the tumour resection. Blinded to the MRE results, the surgeon evaluated the tumour consistency as either soft (softer than white matter), intermediate (similar to white matter), or hard (stiffer than white matter). MRE was 100% accurate at predicting tumour stiffness as decided by the surgeon. Similarly, Murphy *et al* (2013a). assessed 12 patients with Meningioma, typically a benign lesion that arises from the meninges. A quantitative analysis of tumour shear stiffness was used to determine statistical significance. Tumour stiffness determined with MRE significantly correlated with the surgeon's assessment, however an even greater correlation was found when the ratio of tumour stiffness to the surrounding brain tissue was measured ($p = 0.0032$).

Furthermore, a higher resolution MRE protocol was developed and used to assess whether MRE could preoperatively detect intratumoural heterogeneity present within Meningiomas (Hughes *et al* 2015). Data were obtained and analysed to measure heterogeneity for a ROI within the tumour mass. Intraoperative observations regarding softness or hardness were graded on a 5-point scale based on the degree of suction, ultrasonic aspiration, or scissors and cautery. In 15 patients, MRE measurements and intraoperative findings correlated in 67% of tumours ($p = 0.02$), with the correlation perhaps greater if highly vascular or smaller lesions had been excluded.

5.1.2. (ii) MRE for the differential diagnosis of intracranial tumours. MRE has also been investigated as a technique to diagnose the type, grade and malignancy of tumours, as a possible
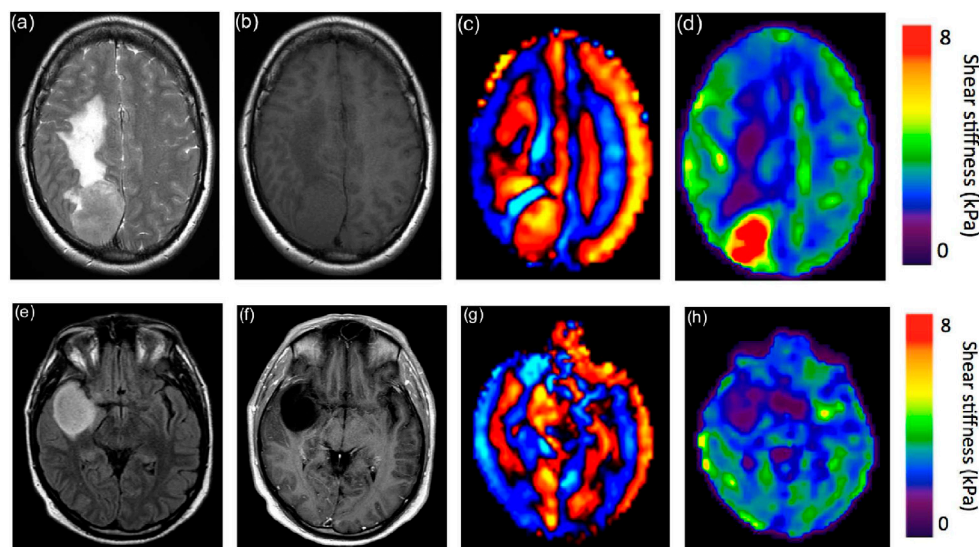
Figure 7. ((a)–(d)) MRI and MRE data from 59 year old female with meningioma. (a) Axial T2-weighted, and (b) T1-weighted image demonstrating the tumour and associated edema, (c) wave image shows longer wavelength throughout the tumour, (d) elastogram shows the tumour to be substantially stiffer, whereas edema is softer, in relation to unaffected tissue. ((e)–(h)) Data from 39 year old male with a glioma (grade IV). (e) T2-weighted and, (f) T1 weighted MRI showing the tumour mass, (g) wave image displays shorter wavelengths in the tumour, (f) elastogram showing the tumour to be softer compared to unaffected brain tissue. Note: elastograms were produced using a direct inversion algorithm at 60Hz.

Table 6. MRE results for glioblastoma multiforme (GBM) and normal appearing white matter (NAWM).

	NAWM	GBM ROI	% difference	p value
$|G^*|$ (kPa)	1.54 ± 0.27	1.32 ± 0.26	-14.29%	$<.001$
ϕ (rad)	0.58 ± 0.07	0.37 ± 0.08	-36.21%	$<.001$

Note. Study by Streitberger *et al* (2014b). Values show means $\pm$ standard deviation.

alternative to routine biopsy procedures used for histological classification. Simon *et al* (2013) analysed a broad range of tumours in 16 patients, including those with meningioma, malignant glioma, anaplastic astrocytoma, and glioblastoma multiforme, among other tumour entities. Using multifrequency MRE and MDEV inversion, malignant tumours presented with a loss of $|G^*|$, when compared to a selected contralateral region of normal appearing white matter (NAWM). Primary brain tumours of the highest malignancy (WHO IV) were more likely to yield soft tissue results, presenting between 33.6–52% softer than NAWM. In addition, the majority of tumours displayed a reduction in the loss tangent ϕ.

A further pilot study which incorporated MDEV inversion, allowed for high-resolution imaging of the viscoelastic properties of a range of tumours in 27 patients (Reiss-Zimmermann *et al* 2014). Supporting findings from Simon *et al* (2013), high grade tumours (WHO Grade IV) were more likely to be softer, as determined by $|G^*|$, and less viscous than those identified as Grade I, II or III. Furthermore, meningioma tumours (Grade I), were on average much stiffer

Table 7. MRE results for global brain tissue (GBT) in MS patients and control participants.

Subtype author	MS-RR Wuerfel *et al* (2010)			MS-CP Streitberger *et al* (2012)		
	Patients	Controls	% difference	Patients	Controls	% difference
N	45	23	—	34	38	—
μ	1.87 ± 0.25	2.14 ± 0.31	-12.7%	2.61 ± 0.48	3.28 ± 0.31	-20.5%
α	0.27 ± 0.01	0.27 ± 0.01	0.3%	0.28 ± 0.01	0.29 ± 0.01	-6.1%

Note. Values represent mean $\pm$ standard deviation (SD).

and displayed higher dissipative behaviour than other tumour entities. See figure 7 for example elastograms of a low grade meningioma (Grade I), and high grade Glioma (Grade IV).

The same protocol was used to assess the mechanical properties of glioblastoma multiforme (GBM), a WHO Grade IV tumour (Streitberger *et al* 2014b). Results from 22 subjects are provided in table 6, for both tumour region and normal appearing white matter (NAWM). GBM was generally softer than healthy tissue, however, 23% of tumours were found to be stiffer than healthy tissue, supporting evidence of high intratumoural variability (Patel *et al* 2014). There was a significant reduction in ϕ in all patients.

5.2. Diffuse diseases

(i) Multiple sclerosis (MS)—MS is a demyelinating disease in which the insulating covers (myelin) of nerve cells in the brain and spinal cord become damaged, with symptoms determined by the location of lesions within white matter. Two studies have used multifrequency MRE and rheological modelling to investigate whether MRE is sensitive to detect known microstructural alterations to the brain in MS. First, Wuerfel *et al* (2010) reported that patients with relapsing-remitting MS (MS-RR) displayed a 13% decrease in μ, ($p < .001$), with no significant changes to α. Second, Streitberger *et al* (2012) found patients with primary or secondary chronic progressive MS (MS-CP), to exhibit a more pronounced reduction in μ (20%) in addition to a significant reduction in α (6%), both ($p < .001$), as shown in table 7.

Clinically isolated syndrome (CIS) is an individual's first episode of neurological symptoms, and may be seen as the precursor to MS due to conversion in 60% of all cases (Alroughani *et al* 2012). CIS diagnosis requires symptoms to last at least 24h and to be caused by inflammation or demyelination in the central nervous system (CNS) in regions such as the spinal cord, brainstem and cerebral hemispheres. Recent research using higher-resolution MDEV-inversion-based multifrequency MRE, reported a 14% reduction in WM stiffness, as characterised by $|G^*|$, in 17 patients compared to 33 healthy control participants ($p < .001$) (Fehlner *et al* 2015). No significant differences in any MRE parameter were found in retrospective analyses between patients who developed MS and those who remained CIS.

(ii) Alzheimer's disease (AD)—AD is a progressive impairment of cognitive function, typically beginning with episodic memory, and is characterised pathologically by extracellular amyloid plaques and intracellular neurofibrillary tangles (McKhann *et al* 1984). Murphy *et al* (2011) found that the stiffness of global brain tissue was decreased in patients with AD compared to age-matched healthy control subjects both with (HC+) and without

Table 8. MRE results for global brain tissue (GBT) in patients with AD, FTD, and control participants.

Author	Population	N	Mean age	Shear stiffness (kPa)	% difference
Murphy *et al* (2011)	AD patients	7	85	2.20 ± 0.13	-7.20%
	HC$-$	14	81.5	2.37 ± 0.12	—
	HC$+$	7	83	2.32 ± 0.13	-5.50%
Huston *et al* (2015)	bvFTD patients	5	60	2.59 ± 0.17	-6.50%
	HC	9	61	2.76 ± 0.08	—

Note. % difference refers to differences between groups of patients and healthy controls in the same study. Values show mean $\pm$ standard deviation (SD).

(HC$-$) significant brain amyloid load, see table 8. More recently, Murphy *et al* (2016) measured the relationship between brain stiffness and severity of AD pathophysiology with 4 groups of subjects including HC$-$, HC $+$, MCI (mild cognitive impairment) and AD. Using the regional MRE processing pipeline, as described in Murphy *et al* (2013b), brain stiffness decreased with increasing AD severity, as determined by existing imaging biomarkers such as hippocampal volume and amyloid load (PIB-SUVR). An optimised meta-region of interest including the frontal, parietal and temporal (FPT) lobes; regions known to be affected by the disease, outperformed all other regions for discriminating between AD patients and healthy control subjects.

(iii) *Fronto-temporal dementia (FTD)*—the behavioural-variant of FTD, (bvFTD), is characterized by prominent changes in personality, interpersonal relationships and conduct, and predominantly involves progressive neuronal loss in the frontal and/or temporal lobes. Specific regions of interest (ROIs) were investigated with MRE due to the well-known localised origin of pathology (Huston *et al* 2015). Using the regional MRE processing pipeline, a specific pattern of brain softening was found in patients with bvFTD in comparison to age matched cognitively healthy participants. A 6.5% decrease was detected in global brain tissue, ($p < .01$), in addition to a 8.5% and 9% decrease in both the frontal lobe ($p < .001$), and temporal lobes ($p < .005$), respectively. No significant differences were found between groups for either the occipital or parietal lobes, deep grey/white matter, cerebellum or the sensory/motor region.

(iv) *Normal pressure hydrocephalus (NPH)*—NPH is a reversible neurological disorder that presents with a triad of clinical symptoms namely, an unusual gait, symptomatic dementia and urinary incontinence. Typical MRI findings are enlargement of the ventricles, while the onset has been attributed to transient intracranial pressure peaks, causing chronic mechanical stress on the ventricular wall. Streitberger *et al* (2010) were the first to study NPH patients with MRE, in order to elucidate whether mechanical changes to brain tissue may play a potential role in the aetiology of the disorder. Assessment of a 2 cm slab of brain tissue, centred through the ventricular region, found μ to be 25% lower in NPH patients, compared to healthy control participants. There was also a significant reduction in α, on the order of 10%, (both $p < .001$), see table 9.

A surgical procedure to relieve some of the symptoms of NPH includes the placement of a ventriculoperitoneal (VP) shunt within the ventricles to drain excess cerebrospinal fluid (CSF). MRE was performed on NPH patients before and after shunt placement to determine the efficacy of treatment and assess mechanical alternations as a result of the intervention (Freimann *et al* 2012). Prior to surgery, a reduction in both μ and α

Table 9. MRE results for global brain tissue (GBT) in NPH patients and control participants.

	N	μ	% difference	α	% difference
Streitberger *et al* (2010)					
Healthy controls	25	2.84 ± 0.088	—	0.287 ± 0.002	—
NPH patients	20	2.27 ± 0.054	-25.1%	0.262 ± 0.002	-9.5%
Freimann *et al* (2012)					
NPH patients pre-shunt	20	2.24 ± 0.085	-26.8%	0.258 ± 0.003	-10%
NPH patients post-shunt	20	2.26 ± 0.092	-25.7%	0.279 ± 0.002	-3%

Note. % difference refers to differences between both groups of patients and healthy controls.
Values show mean $\pm$ standard error (SE).

was found by 27% and 10%, respectively, compared to healthy control data taken from Streitberger *et al* (2010), (both $p < .001$). Post-shunt surgery, patients did not exhibit any changes to μ, with data collected on average 3 months later. However, results for α normalised and returned within 3% of values found for healthy control subjects, ($p < .001$). More recently, Fattahi *et al* (2015) have investigated specific regions of interest (ROIs) in the brain of NPH patients. In contrast to findings from Streitberger *et al* (2010) and Freimann *et al* (2012), patients with NPH were found to exhibit an increase to the brain's shear stiffness, when compared to data collected from age-and-gender-matched controls. An increase in stiffness was apparent in GBT (3.9%), occipital lobe (12%), partietal lobe (12.6%) and temporal lobe (2.6%). No significant differences were found in either the frontal lobe, cerebellum, or deep grey and white matter.

(v) *Parkinson's disease (PD) and progressive supranuclear palsy (PSP)*—PD is characterised by death of dopaminergic neurons in the substantia nigra, which forms part of the basal ganglia, causing tremor, gait difficulty and rigidity. Patients with PSP also display a progressive deterioration in motor function, but pathology instead involves the widespread degeneration of specific axons, particularly in the brainstem, cerebral cortex and basal ganglia. PSP is frequently misdiagnosed as PD because of the shared clinical manifestations, and so therefore MRE was used to to eludicate alternative mechanical profiles to aid in differential diagnosis (Lipp *et al* 2013). Both a 3D direct inversion approach of a volumetric slab of brain tissue, and 2D multi-frequency springpot analysis to model a single image slice, offered enhanced sensitivity to assess regional brain changes in addition to modelling the frequency-independent material properties. Results for GBT are given in table 10, with no significant differences found between PD patients and healthy control participants. In PSP, $|G^*|$, ϕ, μ, α were all reduced for GBT, with μ in particular, undergoing the most statistically significant change, ($p < .001$). Regional analysis of the basal ganglia region in patients with PD detected a significant loss of $|G^*|$ and α in the lentiform nucleus by 6.9% and -7.4%, respectively, ($p < .05$), with PSP patients displaying even greater losses in all four assessed parameters.

(vi) *Amyotrophic lateral sclerosis (ALS)*—the corticospinal tract (CST) consists of nerve fibres that travel from the cerebral cortex and terminate in the spinal cord. Degeneration of the CST has been implicated in ALS, causing progressive and irreversible loss of motor function. Due to the highly anisotropic properties of these fibres, an innovative

Table 10. MRE results for GBT in patients with PD, PSP and control participants.

Subtype	Controls	PD Patients	PD % difference	PSP Patients	PSP % difference
N	18	18	—	16	—
$|G^*|$	1.97 ± 0.042	1.88 ± 0.061	n.s	1.68 ± 0.043	-10.6%
ϕ	0.26 ± 0.009	0.22 ± 0.016	n.s	0.17 ± 0.018	-34.6%
μ	2.79 ± 0.071	3.04 ± 0.191	n.s	1.98 ± 0.126	-28.8%
α	0.30 ± 0.002	0.30 ± 0.005	n.s	0.29 ± 0.003	-4.9%

Note. % difference refers to differences between both groups of patients and healthy controls. Values represent mean and standard deviation (SD) (Lipp *et al* 2013).

approach for measuring the mechanical properties of this structure combines the use of MRE with diffusion tensor imaging (DTI), and anisotropic equations of motion (Romano *et al* 2012)—a technique known as waveguide elastography (WGE). In particular, DTI was used to locate fibre pathways, before the application of spatial-spectral filtering to identify waves that are travelling in a specific direction relative to the fibre orientation. Clinically, this method has been used to assess the stiffness of the CST in 14 patients with ALS in comparison to 14 age-matched healthy controls (Romano *et al* 2014). Analysis of shear waves identified propagating parallel to the principal direction of nerve fibres in the CST, revealed a 5.3% decrease in the shear stiffness in the patient cohort, indicating a significant softening along this tract, ($p < .01$).

6. Discussion

In this review article, we have provided a comprehensive description of the acquisition and analysis methods used in a brain MRE investigation. Second, results for global brain tissue (GBT), grey matter (GM) and white matter (WM) have been standardised and summarised for healthy volunteers. Significantly, we show the ability of MRE to detect changes to the brain in patients with a wide range of focal and diffuse neurological disorders. In the following section, we will describe how these findings relate to neuroanatomy, and suggest explanations for anomalies found within the literature. In addition, we will review the implications of clinical findings and how MRE results may relate to pathophysiology. Finally, we will discuss the research that is ongoing to further develop the MRE acquisition and analysis technique and discuss the potential applications of MRE within neuroscience.

6.1. Summary of results from healthy participants

Comparing mechanical property measurements across different studies and research groups is often cumbersome, due to the reporting of a wide-range of MRE-derived variables. Conducting a systematic literature search allowed us to obtain a comprehensive list of brain MRE results. Through the conversion of values to common parameters of shear stiffness and loss tangent, we have standardised the mean values obtained for healthy volunteers, in order to provide reference values for GBT, GM and WM, see tables 3 and 4, respectively. We should, however, mention that subject age is also likely to contribute to variations to mechanical properties, as reported in a number of studies (Sack *et al* 2009, 2011, Arani *et al* 2015). For the purpose of this review, we have instead focused on the effect of mechanical frequency on MRE

measurements, as frequency is likely to be more influential on the variation in results apparent across the literature.

Shear stiffness values for GBT range between 0.62–3.70 kPa, with a mean value of 2.07 kPa at 50 Hz. Lower stiffness values are apparent at lower frequencies, which can be attributed to the fact that biological tissue exhibits a frequency-dependent response (Szabo and Wu 2000). We have therefore quantified the change in brain stiffness due to the mechanical frequency. On average, we find that with every 10 Hz increase in frequency, there is a 0.4 kPa increase in shear stiffness. Studies that employ alternative frequencies should bear this in mind when making comparisons with other research groups.

Calculation of the loss tangent ϕ for GBT was possible in 6 studies, where values range between 0.09 rad–0.70 rad. At 50 Hz, the mean value is 0.41 rad. There is clearly a wide disparity in values, which may be attributed to variation in frequency and MRE methodology. For example, Dittmann *et al* (2015) used low frequencies for MDEV inversion (10–20 Hz) and a revised calculation of ϕ to account for systemic noise bias and tissue heterogeneities. The new calculation of ϕ was 0.09 rad, and the authors suggest that previous work from their group may have provided values that were overestimated (Braun *et al* 2014, Guo *et al* 2012).

Nine out of 10 studies report that WM is stiffer than GM. This difference is interpreted to be due to the fact that WM primarily consists of tightly aligned myelinated highly orientated axons, whereas grey matter is largely composed of cell bodies, unmyelinated axons and neuroglia (Holland *et al* 2015). Green *et al* (2008) was the sole study to report that GM is stiffer than WM. Potential explanations for this anomaly include the utilisation of a bite-bar actuator, which may not be effective at transmitting waves into the very centre of the brain, with low motion affecting SNR and resulting measurements. Interestingly, it has been suggested that cell body density has a larger impact on local tissue stiffness than cell stiffness itself (Koser *et al* 2015). The fact that MRE reports greater WM stiffness is not surprising as WM fibres are dense and compact. In contrast, GM has been found to be stiffer than WM on an individual cell level (Lu *et al* 2006). GM contains more (stiffer) neuronal cell bodies that WM, whereas WM is dominated by softer neuronal and glial cell processes; thus on alternative scales, mechanical properties of tissue may vary.

We find the shear stiffness of GM to range between 1.03 kPa–5.30 kPa, and between 1.27 kPa–13.60 kPa for WM. At 50 Hz, mean GM stiffness is 2.29 kPa and WM stiffness is 3.21 kPa, equating to WM being approximately 40% stiffer than GM. Appreciably higher shear stiffness values were obtained by Kruse *et al* (2008) compared to all other studies, even when taking into consideration the higher mechanical frequency of 100 Hz. Stiffness of GM was 5.22 kPa and 13.60 kPa for WM. The higher measurements have been attributed to the 2D LFE inversion technique, which may not have been optimised to minimize through-plane wave propagation. Through-plane propagating waves can appear in 2D data as waves with longer wavelengths, thus overestimating tissue stiffness (Murphy *et al* 2011). Furthermore, lower shear stiffness values are notable in a study by Braun *et al* (2014), who utilised multi-frequency MRE and MDEV inversion. Stiffness of GM was 0.98 kPa and 1.16 kPa for WM. Direct comparison of values with the shear stiffness reported by other groups is not possible because of the inherent frequency averaging implied by MDEV inversion, and greater contribution of the lower frequency images due to naturally higher amplitudes (Guo *et al* 2013). This study also utilised an MRI scanner at 7 T. Field-strength *per se* is not expected to influence MRE measurements (Hamhaber *et al* 2007), however, improved image resolution may improve the ability for MRE to detect fine features and thus alter the sinusoidal wave profile.

Storage and loss moduli were provided for GM and WM in 6 out of the 10 studies, enabling the calculation of the loss tangent. GM was less viscous than WM in all of the studies identified, with GM results ranging between 0.37 rad–0.95 rad, and WM values ranging between

0.46 rad–1.03 rad. Higher WM viscosity, relative to GM, indicates that the microstructure of WM has a highly complex structure and supports recent *in vitro* findings that measured both stress relaxation and relaxation times in both types of tissue (Budday *et al* 2015). In addition, higher WM viscosity is also consistent with the microstructural architecture of GM and WM, and found to reflect the network properties of WM found at the macromolecular level (Franceschini *et al* 2006). Particularly high values for the loss tangent are evident in Braun *et al* (2014), with 0.95 rad for GM and 1.03 rad for WM. As previously mentioned, these values are likely to have been overestimated due to systemic noise bias; subsequent work has focused on the recalculation of $\phi*$ (Dittmann *et al* 2015). Nonetheless, the original parameter was reported as sensitive to a variety of pathological processes, as described in both Streitberger *et al* (2014b) and Reiss-Zimmermann *et al* (2014).

An increasing number of studies have investigated regional mechanical properties, including anatomical brain structures. Comparison of all four lobes of the brain found the parietal lobe to be the softest lobe, with conflicting information finding either the temporal and occipital lobes to be the stiffest lobar region. Whether lobar variation in stiffness is explained by fundamental brain architectural differences has not yet been determined, and is the subject of future investigations. Interesting to note is the consistent relationship between values for each lobar region across studies that followed the same protocol, see table 5. Variation in the values seen across studies may be attributed to the mean age of subjects, lending support to studies that suggest increasing age may contribute to a loss of brain stiffness (Sack *et al* 2009, 2011, Arani *et al* 2015). Softer GM and WM of the cerebellum relative to the corresponding compartments of the cerebrum may be attributed to the cerebellar surface being comprised of thin layers of tissue with finely spaced parallel grooves, thus displaying a finer microstructure compared to the broad irregular convolutions of the cerebral cortex. Finally, the corticospinal tract (CST) was determined to be twice as stiff as general brain tissue, which may be attributed to the fact that the majority of CST axons are myelinated.

6.2. Summary of clinical findings

MRE has shown great promise as a non-invasive imaging modality to assess the mechanical properties of intracranial tumours. Highly consistent results were found relating shear stiffness measurements with the manual palpation experience of the neurosurgeon during surgery. Importantly, tumour stiffness measured by MRE outperformed predictions from conventional MRI using T1 and T2-weighted images (Murphy *et al* 2013a). MRI has previously found soft tumours to be hyperintense and less likely to be associated with edema on T2 images (Hoover *et al* 2011). However, conventional MRI could only accurately predict the softest and hardest meningiomas prior to surgical resection, with little success determining the tumour consistency between the two extremes. Furthermore, the importance of using a high-resolution MRE protocol becomes apparent when seeking to obtain a full and more accurate understanding of the internal variation in stiffness within tumours (Hughes *et al* 2015). Future studies should aim to assess specific regions within the tumour mass to more accurately define intrinsic mechanical heterogeneity to enhance the potential utility of MRE as a pre-surgical tool. Measurement of tumour stiffness should also be normalised to surrounding brain tissue, as a result of intrasubject variability in presumably unaffected brain tissue (Murphy *et al* 2013a).

Investigations into the use of MRE as a technique for the differential diagnosis of brain tumours, suggest that more malignant tumours, determined by WHO classification, are more likely to be less stiff, as determined by $|G^*|$, and display a reduction in the loss tangent ϕ. While a uniform reduction in $|G^*|$ is interpreted as a weakening or softening of the mechanical

rigidity of tissue, an alteration of the loss tangent ϕ is interpreted as a more severe degradation of the tissue structure due to a change in the complexity of the tissue architecture (Sack *et al* 2013). In contrast, Meningioma tumours were the only tumour entity to display increased stiffness, $|G^*|$, and a highly cross-linked architecture ϕ. This may be attributed to the initial development of pathology in the meninges, which is comprised of a thick layer of dura mater, arachnoid mater, and pia mater, in addition to their propensity to calcify.

The majority of neurodegenerative diseases are accompanied by significant and widespread softening of brain tissue. This is contradictory to what was initially hypothesised in patients with Alzheimer's disease (AD), with the aggregation of stiff amyloid protein expected to lead to an increase in tissue stiffness (Murphy *et al* 2011). On reflection, patients recruited into this study had a clinical diagnosis of AD, at which stage significant neurodegeneration is likely. Interestingly, a recent study has found the relationship between brain stiffness and AD severity to be non-linear and non-monotonic (Murphy *et al* 2016), suggesting that brain stiffness spikes at the onset of MCI, before falling to levels observed in AD during the later stages of MCI. This would appear to support the theory that the initial development of amyloid protein is associated with increased brain stiffness, before a decrease in brain stiffness due to wide-spread cell death and a loss of tissue integrity. Further investigations are warranted to corroborate that other aspects of the AD pathological cascade follow the same trajectory and to link MRE results with histological samples. Complementing these findings, patients with frontal-temporal dementia (FTD) also exhibited a significant loss in brain stiffness in the frontal and temporal lobes, where neurodegeneration is known to originate (Seelaar *et al* 2011). As the same MRE protocol was used, the difference in brain stiffness between the AD and FTD healthy control subjects, as shown in table 8, is most likely due to subject age with the AD control group approximately 20 years senior.

Patients with early or chronic MS has shown how disease severity can influence mechanical property measurements. In the early stages of MS (MS-RR), the strength of the brain is degraded, as indicated by μ, while the geometrical arrangement α remains intact. To complement these findings, the underlying cellular and molecular mechanisms behind these changes were examined in two mouse models of MS. In the first study, mice were fed copper chelator cuprizone to induce reversible demyelination (Schregel *et al* 2012). Histopathological analyses were correlated with MRE measurements, and found that the magnitude of the complex shear modulus $|G^*|$ decreased with extensive demyelination and extracellular matrix degradation (Schregel *et al* 2012). In addition, experimental autoimmune encephaomyelitus (EAE) was induced in mice to further investigate the relationship between viscoelasticity and inflammation (Riek *et al* 2012). A reduction in both the storage and loss moduli was found at the peak of the disease, and attributed to the amount of focal inflammation during EAE. There was no significant change to the loss tangent φ indicating that inflammation affects stiffness independently to alterations in tissue architecture—supporting human patient findings from Wuerfel *et al* (2010). On the other hand, patients with chronic MS (MS-CP), were found to exhibit even softer brains than patients with MS-RR, as determined by μ, as well as a less complex geometrical arrangement indicated by a significant loss to α. Deficits due to MS-CP are considered irreversible due to progressive neurodegeneration, and thus may explain the more drastic changes to the alignment of the tissue network, although to date, animal models of MS-CP have not been combined with MRE and histopathology. The need for standardisation across and within research groups becomes apparent when comparing the mechanical properties between MS-RR and MS-CP directly. Changes in the protocol between studies and in particular, the limits of bandpass filtering, have resulted in different base-line values for healthy control subjects. Nevertheless, the application of MRE to investigate patients with

early or chronic MS, has shown how disease severity can differentially effect mechanical property measurements, thereby showing potential as a unique marker of disease progression.

Patients with NPH has shown how MRE is sensitive for detecting alterations to the brain as a result of surgical intervention. In the first instance, Streitberger *et al* (2010) and Freimann *et al* (2012) found patients with NPH to display a decrease in both μ and α parameters. However, with shunt intervention, α values were found to normalise and return within the range obtained for the comparison group of healthy control subjects. The fact that μ remained unchanged supports the notion that spring-pot parameters represent two independent processes. Shunt placement was associated with reordering the geometry alignment of the mechanical scaffold of the brain, without influencing cellular strength or connectivity. On the contrary, Fattahi *et al* (2015) reported an *increase* to the shear stiffness in the cerebrum (GBT), and in a number of lobar regions in NPH patients. An increase in brain stiffness may be caused by the dilation of the ventricles, leading to brain tissue compression. Resulting cellular alterations are likely to create a higher tissue-to-fluid ratio within the cerebrum. Importantly, the discrepancy in findings between studies has been attributed to the use of alternative protocols (Fattahi *et al* 2015). One example is that Streitberger *et al* (2010) and Freimann *et al* (2012) utilised modelling to specifically assess a small slab of tissue near the ventricular region. On the contary, Fattahi *et al* (2015) obtained full brain-coverage to assess specific and larger regions of interest; however, it is possible that alternative brain regions will undergo disparate changes throughout the NPH process.

MRE may also assist in differential diagnosis, as was evident in the study of PD and PSP patients. Misdiagnosis is common, due to similar and overlapping symptoms, however MRE results indicate that PD and PSP have distinct mechanical profiles. PD patients displayed significant changes to $|G^*|$ and α during an assessment of the basal ganglia region; no significiant changes were detected in GBT. PD pathology involves presynaptic accumulation of α-synuclein which starts focally and affects axonal integrity only later in the process of degeneration (Schulz-Schaeffer 2010), and thus may explain why changes to GBT were not detected. In contrast, PSP patients displayed pronounced changes in $|G^*|$, ϕ, μ and α, both globally and in the basal ganglia. PSP typically involves an early loss of neuronal axons, which are essential in maintaining brain tissue integrity. This study highlights the importance of investigating a specific brain structure associated with a particular disorder. If the basal ganglia hadn't been investigated, PD patients would not have been differentiated from healthy control participants.

Finally, the use of wave-guide elastography (WGE) found a significant softening of the corticospinal tract (CST) in patients with amyotrophic lateral sclerosis (ALS). This technique may prove to be valuable in the diagnosis of ALS, although further clinical trials are required. The combination of histological analyses with MRE measurements will be imperative in order to relate pathological cellular changes to MRE constants. The use of WGE is unlikely to be useful for the assessment of tissue stiffness among other brain regions. WGE analysis is reliant on knowledge of the pathways along which the propagating waves will travel, however, most brain structures or regions do not possess anisotropic properties on the same scale as the CTS.

6.3. Summary of the brain MRE technique

There has been enormous growth in the abilities to perform brain MRE, but significant advances are necessary. Future work to enhance the clinical utility of brain MRE include identifying the preferred mechanical actuator for patients, with recent work concluding that a remote device was preferable to the head-cradle (Fehlner *et al* 2015). Calculation of the

strain-based signal-to-noise ratio (i.e. OSS-SNR) (McGarry *et al* 2011) from a number of actuators, while assessing patient comfort and operator convenience, will assist in the determination of the optimal arrangement. A reduction in acquisition time would also be an important clinical advance and could potentially increase patient acceptance. A multidirectional motion encoding scheme, known as sample interval modulation (SLIM), was found to produce nearly identical elastograms compared with a conventional MRE encoding scheme, albeit 2.5 times faster (Klatt *et al* 2015). This technical development may also provide an opportunity to capture additional displacement data, and could increase repeatability due to the lower risk of subject motion.

Since the majority of brain disorders have localised regions of origin, it is critical to further develop the spatial resolution of MRE in order to more accurately measure the mechanical properties of smaller brain structures that correspond to differences in anatomy. This can be made possible either through data acquisiton or data analysis procedures. For example, the development of the multi-shot multi-slab spiral sequence has enabled MRE data to be obtained at resolution of 1.6 mm, allowing the reliable measurement of subcortical grey matter structures (Johnson *et al* 2016). In addition, for the first time, MRE has been combined with the stationary super-resolution (SSR) technique, in which multiple lower-resolution images from the same scene are interpolated and fused to create a single higher-resolution image (Elad and Feuer 1997). The Elastography Software Pipeline (ESP) is a new analysis tool that combines SSR with multifrequency MRE to spatially resolve sub-voxel features, resulting in a new level of radiological detail (Barnhill *et al* 2016). Example elastograms from this pipeline are provided in figure 1.

Beyond the scope of currently available techniques, it is important to consider that the frequency-dependence of tissue may provide useful diagnostic information in itself. Gathering information over a range of frequencies to assess how tissue is differentially affected under varying forces/strains, is likely to be of clinical interest. In addition, further advances in NLI techniques to fully validate the use of more sophisticated tissue models such as poroelasticity is also likely to provide further clinically relevant information (Perrinez *et al* 2010, McGarry *et al* 2015). Methodological developments targeting the reconstruction of anisotropic mechanical properties will also be welcomed given recent findings that alternative displacement fields reveal significantly different mechanical values, particularly in highly aligned white matter regions (Anderson *et al* 2016). With the application of more elaborate mechanical models, it may also be possible to improve the specificity of MRE to discriminate between specific pathologies such as inflammation, degeneration and edema.

Whether brain MRE can provide *accurate* quantitative values for mechanical properties will be difficult to determine. Indentation methods can reliably record the stiffness of, for example, grey and white matter (Budday *et al* 2015), but it remains an *ex vivo* technique that cannot predict the mechanical characteristics of living brain tissue *in situ*. Nevertheless, it is promising that brain MRE values have converged to the same order of magnitude as those seen in conventional mechanical testing. In fact, recent work with low frequency MRE has seen remarkable agreement with data obtained with shear-oscillatory rheometry, and may be seen as the missing link between static test methods and conventional *in vivo* MRE (Dittmann *et al* 2015).

On the other hand, accurate mechanical values *per se* may be less important than the determination of the most clinically sensitive and reliable protocol. More studies have been reporting repeatability values, with promising results (Johnson *et al* 2013a, 2016, Murphy *et al* 2013b, Anderson *et al* 2016). For example, Murphy *et al* (2013b) report that their MRE processing pipeline possesses a typical coefficient of variation of <1% for global brain stiffness, and <2% for regional lobe stiffness measurements. At a higher 1.6 mm spatial resolution, Johnson *et al* (2016) report a coefficient of variation of 1–2% for global measures, and 3–7%

for measures of subcortical grey matter structures. Future work should continue to provide repeatability and SNR measurements to enable cross-centre comparisons.

As illustrated by this review, providing standardised baseline values for brain is currently very challenging, and values provided for a clinical cohort will only be relevant to those who follow the same methodology. Determination of a standardised protocol and agreement in baseline values for healthy subjects, as seen in liver MRE and in the staging of fibrosis, is required. Only in this case can the true sensitivity of brain MRE be realised.

6.4. Applications in neuroscience

Recent research in the clinical brain sciences has shifted towards disease prevention, and the development of techniques for early diagnosis. With further advances in the MRE technique, brain MRE has the potential to make an impact in this specialty. Most obvious is the application of MRE for the detection of early pathological changes to specific brain structures in individuals who may be asymptomatic, but in the prodromal stages of a range of organic brain disorders. Mechanical alterations to the hippocampus, for example, may be useful in detecting the early stages of Alzheimer's disease. This is supported, in particular, by a recent study by Schwarb *et al* (2016), who reported a high correlation between MRE hippocampal damping ratio and memory performance in healthy young adults. There is also the possibility of assessing regions that are initially affected in a range of other dementias such as dementia with Lewy bodies, and Creutzfeldt–Jakob disease, to aid in differential diagnosis and determine the most appropriate medical intervention. To our knowledge, MRE has not been applied to the study of psychiatric disorders, and therefore the potential utility remains unknown. Further research should also bridge the disciplines within neuroscience and create developmental models of diseases that link mechanical properties to genetic, cellular and biochemical observations.

7. Conclusion

An increasing body of research has now investigated the use of MRE to study the mechanical properties of the human brain *in vivo*. Recent advances in image acquisition and analysis have allowed study of the biomechanics of the brain in unprecedented detail. The development of a standardised brain MRE protocol, and thus establishing normative and importantly, reliable values of brain tissue stiffness, is now necessary before large-scale clinical investigations. MRE holds promise to be a valuable imaging tool to diagnose, monitor and evaluate pharmaceutical strategies in a host of neurological disorders.

While MRE packages for examining the liver are currently available from all major MRI vendors, EPI-based sequences for brain MRE should be available in the near future.

Acknowledgments

References

Alroughani R, Al Hashel J, Lamdhade S and Ahmed S F 2012 Predictors of conversion to multiple sclerosis in patients with clinical isolated syndrome using the 2010 revised McDonald criteria *ISRN Neurol.* **2012** 792192

Anderson A T, Van Houten E E W, McGarry M D J, Paulsen K D, Holtrop J L, Sutton B P, Georgiadis J G and Johnson C L 2016 Observation of direction-dependent mechanical properties in the human brain with multi-excitation MR elastography *J. Mech. Behav. Biomed. Mater.* **59** 538–46

Arani A, Da Rosa M, Ramsay E, Plewes D B, Haider M A and Chopra R 2013 Incorporating endorectal MR elastography into multi-parametric MRI for prostate cancer imaging: initial feasibility in volunteers *J. Magn. Reson. Imaging* **38** 1251–60

Arani A, Murphy M C, Glaser K J, Manduca A, Lake D S, Kruse S A, Jack C Jr, Ehman R K and Huston J 3rd 2015 Measuring the effects of aging and sex on regional brain stiffness with MR elastography in healthy older adults *Neuroimage* **111** 59–64

Asbach P, Klatt D, Hamhaber U, Braun J, Somasundaram R, Hamm B and Sack I 2008 Assessment of liver viscoelasticity using multifrequency MR elastography *Magn. Reson. Med.* **60** 373–9

Asbach P *et al* 2010 Viscoelasticity-based staging of hepatic fibrosis with multifrequency MR elastography *Radiology* **257** 80–6

Barnhill E, Hollis L, Sack I, Braun J, Hoskins P R, Pankaj P, Brown C, van Beek E J R and Roberts N 2016 Nonlinear multiscale regularisation in MR elastography: towards fine feature mapping *Med. Image Anal.* **35** 133–45

Barnhill E, Kennedy P, Johnson C, Mada M and Roberts N 2015 Real-time 4D phase unwrapping applied to magnetic resonance elastography *Magn. Reson. Med.* **73** 2321–31

Bensamoun S F, Ringleb S I, Chen Q, Ehman R L, An K and Brennan M 2007 Thigh muscle stiffness assessed with magnetic resonance elastography in hyperthyroid patients before and after medical treatment *J. Magn. Reson. Imaging* **26** 708–13

Bensamoun S F, Ringleb S I, Littrell L, Chen Q, Brennan M, Ehman R L and An K 2006 Determination of thigh muscle stiffness using magnetic resonance elastography *J. Magn. Reson. Imaging* **23** 242–7

Bensamoun S F, Robert L, Leclerc G E, Debernard L and Charleux F 2011 Stiffness imaging of the kidney and adjacent abdominal tissues measured simultaneously using magnetic resonance elastography *Clin. Imaging* **35** 284–7

Braun J, Guo J, Lützkendorf R, Stadler J, Papazoglou S, Hirsch S, Sack I and Bernarding J 2014 High-resolution mechanical imaging of the human brain by three-dimensional multifrequency magnetic resonance elastography at 7 T *Neuroimage* **90** 308–14

Brock M, Löppenberg B, Roghmann F, Pelzer A, Dickmann M, Becker W, Martin-Seidel P, Sommerer F, Schenk L, Palisaar R J, Noldus J and von Bodman C 2015 Impact of real-time elastography on magnetic resonance imaging/ultrasound fusion guided biopsy in patients with prior negative prostate biopsies *J. Urol.* **193** 1191–7

Budday S, Nay R, de Rooij R, Steinmann P, Wyrobek T, Ovaert T C and Kuhl E 2015 Mechanical properties of gray and white matter brain tissue by indentation *J. Mech. Behav. Biomed. Mater.* **46** 318–30

Burlew M M, Madsen E L, Zagzebski J A, Banjavic R A and Sum S W 1980 A new ultrasound tissue-equivalent material *Radiology* **34** 517–20

Chakraborty A, Bamber J C and Dorward N L 2012 Preliminary investigation into the use of ultrasound elastography during brain tumour resection *Ultrasound* **20** 33–40

Chen Q, Basford J and An K 2008 Ability of magnetic resonance elastography to assess taut bands *Clin. Biomech.* **23** 623–9

Clayton E H, Genin G M and Bayly P V 2012 Transmission, attenuation and reflection of shear waves in the human brain *J. R. Soc. Interface* **9** 2899–910

Dittmann F, Hirsch S, Tzschätzsch H, Guo J, Braun J and Sack I 2015 *In vivo* wideband multifrequency MR elastography of the human brain and liver *Magn. Reson. Med.* **76** 1116–26

Doyley M M and Parker K J 2014 Elastography: general principles and clincial applications *Ultrasound Clin.* **9** 1–11

Edelman R R and Warach S 1993 Magnetic resonance imaging *N. Engl. J. Med.* **328** 708–16

Ehman E C, Rossman P J, Kruse S A, Sahakian A V and Glaser K J 2008 Vibration safety limits for magnetic resonance elastography *Phys. Med. Biol.* **53** 925–35

Elad M and Feuer A 1997 Restoration of a single superresolution image from several blurred, noisy, and undersampled measured images *Trans. Imag Proc.* **6** 1646–58

Elgeti T, Beling M, Hamm B, Braun J and Sack I 2010 Cardiac magnetic resonance elastography: toward the diagnosis of abnormal myocardial relaxation *Invest. Radiol.* **45** 782–7

Fattahi N, Arani A, Perry A, Meyer F, Manduca A, Glaser K, Senjem M L, Ehman R L and Huston J 2015 MR elastography demonstrates increased brain stiffness in normal pressure hydrocephalus *AJNR Am. J. Neuroradiol.* **37** 462–7

Fehlner A, Behrens J R, Streitberger K-J, Papazoglou S, Braun J, Bellmann-Strobl J, Ruprecht K, Paul F, Wurfel J and Sack I 2016 Higher-resolution MR elastography reveals early mechanical signatures of neuroinflammation in patients with clinically isolated syndrome *J. Magn. Reson. Imaging* **44** 51–8

Fehlner A, Papazoglou S, McGarry M D, Paulsen K D, Guo J, Streitberger K J, Hirsch S, Braun J and Sack I 2015 Cerebral multifrequency MR elastography by remote excitation of intracranial shear waves *NMR Biomed.* **28** 1426–32

Franceschini G, Bigoni D, Regitnig P and Holzapfel G 2006 Brain tissue deforms similarly to filled elastomers and follows consolidation theory *J. Mech. Phys. Solids* **54** 2592–620

Freimann F B, Muller S, Streitberger K, Guo J, Rot S, Ghori A, Vajkoczy P, Reiter R, Sack I and Braun J 2013 MR elastography in a murine stroke model reveals correlation of macroscopic viscoelastic properties of the brain with neuronal density *NMR Biomed.* **26** 1534–9

Freimann F B, Streitberger K, Klatt D, Lin K, McLaughlin J, Braun J, Sprung C and Sack I 2012 Alteration of brain viscoelasticity after shunt treatment in normal pressure hydrocephalus *Neuroradiology* **54** 189–96

Goss B C, McGee K P, Ehman E C, Manduca A and Ehman R L 2006 Magnetic resonance elastography of the lung: technical feasibility *Magn. Reson. Med.* **56** 1060–6

Green M A, Bilston L E and Sinkus R 2008 *In vivo* brain viscoelastic properties measured by magnetic resonance elastography *NMR Biomed.* **21** 755–64

Guo J, Hirsch S, Fehlner A, Papazoglou S, Scheel M, Braun J and Sack I 2013 Towards an elastographic atlas of brain anatomy *PLoS One* **8** e71807

Guo J, Posnansky O, Hirsch S, Scheel M, Taupitz M, Braun J and Sack I 2012 Fractal network dimension and viscoelastic powerlaw behavior: II. An experimental study of structure-mimicking phantoms by magnetic resonance elastography *Phys. Med. Biol.* **57** 4041–53

Hamhaber U, Sack I, Papazoglou S, Rump J, Klatt D and Braun J 2007 Three-dimensional analysis of shear wave propagation observed by *in vivo* magnetic resonance elastography of the brain *Acta. Biomater.* **3** 127–37

Hatt A, Cheng S, Tan K, Sinkus R and Bilston L E 2015 MR elastography can be used to measure brain stiffness changes as a result of altered cranial venous drainage during jugular compression *AJNR Am. J. Neuroradiol.* **36** 1971–7

Herráez M A, Burton D R, Lalor M J and Gdeisat M A 2002 Fast two-dimensional phase-unwrapping algorithm based on sorting by reliability following a noncontinuous path *Appl. Opt.* **41** 7437–44

Holland M A, Miller K E and Kuhl E 2015 Emerging brain morphologies from axonal elongation *Ann. Biomed. Eng.* **43** 1640–53

Hoover J M, Morris J M and Meyer F B 2011 Use of preoperative magnetic resonance imaging T1 and T2 sequences to determine intraoperative meningioma consistency *Surg. Neurol. Int.* **2** 142

Hughes J D, Fattahi N, Van Gompel J, Arani A, Lanzino G, Link M, Meyer F, Ehman R and Huston J 3rd 2015 Higher resolution magnetic resonance elastography for the evaluation of intratumoral heterogeneity in meningiomas *J. Neurol. Surg.* B **76** A139

Huston J, Murphy M C, Boeve B F, Fattahi N, Arani A, Glaser K J, Manduca A, Jones D T and Ehman R L 2015 Magnetic resonance elastography of frontotemporal dementia *J. Magn. Reson. Imaging* **43** 474–8

Johnson C L, Holtrop J L, McGarry M D J, Weaver J B, Paulsen K D, Georgiadis J G and Sutton B P 2014 3D multislab, multishot acquisition for fast, whole-brain MR elastography with high signal-to-noise efficiency *Magn. Reson. Med.* **71** 477–85

Johnson C L, McGarry M D J, Gharibans A A, Weaver J B, Paulsen K D, Wang H, Olivero W C, Sutton B P and Georgiadis J G 2013a Local mechanical properties of white matter structures in the human brain *Neuroimage* **79** 145–52

Johnson C L, McGarry M D J, Van Houten E E W, Weaver J B, Paulsen K D, Sutton B P and Georgiadis J G 2013b Magnetic resonance elastography of the brain using multishot spiral readouts with self-navigated motion correction *Magn. Reson. Med.* **70** 404–12

Johnson C L, Schwarb H, McGarry M D J, Anderson A T, Huesmann G R, Sutton B P and Cohen N J 2016 Viscoelasticity of subcortical gray matter structures *Hum. Brain Mapp.* **37** 4221–33

Klatt D, Hamhaber U, Asbach P, Braun J and Sack I 2007 Noninvasive assessment of the rheological behavior of human organs using multifrequency MR elastography: a study of brain and liver viscoelasticity *Phys. Med. Biol.* **52** 7281

Klatt D, Johnson C L and Magin R 2015 Simultaneous, multidirectional acquisition of displacement fields in magnetic resonance elastography of the *in vivo* human brain *J. Magn. Reson. Imaging* **42** 297–304

Knutsson H, Westin C F and Granlund G 1994 Local multiscale frequency and bandwidth estimation *Proc. of 1st Int. Conf. on Image Processing* pp 36–40

Kolipaka A, McGee K P, Araoz P A, Glaser K J, Manduca A, Romano A J and Ehman R L 2009 MR elastography as a method for the assessment of myocardial stiffness: comparison with an established pressure-volume model in a left ventricular model of the heart *Magn. Reson. Med.* **62** 135–40

Koser D E, Moeendarbary E, Hanne J, Kuerten S and Franze K 2015 CNS cell distribution and axon orientation determine local spinal cord mechanical properties *Biophys. J.* **108** 2137–47

Kruse S A, Rose G H, Glaser K J, Manduca A, Felmlee J P, Jack C R Jr and Ehman R L 2008 Magnetic resonance elastography of the brain *Neuroimage* **39** 231–7

Lipp A, Trbojevic R, Paul F, Fehlner A, Hirsch S, Scheel M, Noack C, Braun J and Sack I 2013 Cerebral magnetic resonance elastography in supranuclear palsy and idiopathic Parkinson's disease *Neuroimage Clin.* **3** 381–7

Loomba R *et al* 2014 Magnetic resonance elastography predicts advanced fibrosis in patients with nonalcoholic fatty liver disease: a prospective study *Hepatology* **60** 1920–8

Lu Y *et al* 2006 Viscoelastic properties of individual glial cells and neurons in the CNS *Proc. Natl Acad. Sci. USA* 103 17759–64

Manduca A, Muthupillai R, Rossman P J, Greenleaf J F and Ehman R L 1996 Image processing for magnetic-resonance elastography *Proc. SPIE* **2710** 616–23

Manduca A, Oliphant T E, Dresner M A, Mahowald J L, Kruse S A, Amromin E, Felmlee J P, Greenleaf J F and Ehman R L 2001 Magnetic resonance elastography: non-invasive mapping of tissue elasticity *Med. Image Anal* **5** 237–54

Mariappan Y K, Glaser K J and Ehman R L 2010 Magnetic resonance elastography: a review *Clin. Anat.* **23** 497–511

Mariappan Y K, Glaser K J, Levin D L, Vassallo R, Hubmayr R D, Mottram C, Ehman R L and McGee K P 2014 Estimation of the absolute shear stiffness of human lung parenchyma using 1H spin echo, echo planar MR elastography *J. Magn. Reson. Imaging* **40** 1230–7

McCracken P J, Manduca A, Felmlee J and Ehman R L 2005 Mechanical transient-based magnetic resonance elastography *Magn. Reson. Med.* **53** 628–39

McGarry M D J, Johnson C L, Sutton B P, Georgiadis J G, Van Houten E E W, Pattison A J, Weaver J B and Paulsen K D 2015 Suitability of poroelastic and viscoelastic mechanical models for high and low frequency MR elastography *Med. Phys.* **42** 947–57

McGarry M D J and Van Houten E E W 2008 Use of a Rayleigh damping model in elastography *Med. Biol. Eng. Comput.* **46** 759–66

McGarry M D J, Van Houten E E W, Johnson C L, Georgiadis J G, Sutton B P, Weaver J B and Paulsen K D 2012 Multiresolution MR elastography using nonlinear inversion *Med. Phys.* **39** 6388–96

McGarry M D J, Van Houten E E W, Perrinez P R, Pattison A J, Weaver J B and Paulsen K D 2011 An octahedral shear strain-based measure of SNR for 3D MR elastography *Phys. Med. Biol.* **56** N153–64

McKhann G, Drachman D, Folstein M, Katzman R, Price D and Stadlan E M 1984 Clinical diagnosis of Alzheimer's disease: report of the NINCDS-ADRDA Work Group under the auspices of Department of Health and Human Services Task Force on Alzheimer's Disease *Neurology* **34** 939–44

Murphy M C, Huston J 3rd, Glaser K J, Manduca A, Meyer F B, Lanzino G, Morris J M, Felmlee J P and Ehman R L 2013a Preoperative assessment of meningioma stiffness using magnetic resonance elastography *J. Neurosurg.* **118** 643–8

Murphy M C, Huston J 3rd, Jack J C, Glaser K J, Manduca A, Felmlee J P and Ehman R L 2011 Decreased brain stiffness in Alzheimer's disease determined by magnetic resonance elastography *J. Magn. Reson. Imaging* **34** 494–8

Murphy M C, Huston J 3rd, Jack J C, Glaser K J, Senjem M L, Chen J, Manduca A, Felmlee J P and Ehman R L 2013b Measuring the characteristic topography of brain stiffness with magnetic resonance elastography *PLoS One* **8** e81668

Murphy M C, Jones D T, Jack C R, Glaser K J, Senjem M L, Manduca A, Felmlee J P, Carter R E, Ehman R L and Huston J 2016 Regional brain stiffness changes across the Alzheimer's disease spectrum *NeuroImage: Clin.* **10** 283–90

Muthupillai R and Ehman R L 1996 Magnetic resonance elastography *Nat. Med.* **2** 601–3

Muthupillai R, Lomas D J, Rossman P J, Greenleaf J F, Manduca A and Ehman R L 1995 Magnetic resonance elastography by direct visualization of propagating acoustic strain waves *Science* **269** 1854–7

Oliphant T E, Manduca A, Ehman R L and Greenleaf J F 2001 Complex-valued stiffness reconstruction for magnetic resonance elastography by algebraic inversion of the differential equation *Magn. Reson. Med.* **45** 299–310

Ophir J, Alam S K, Garra B, Kallel F, Konofagou E, Krouskop T and Varghese T 1999 Elastography: ultrasonic estimation and imaging of the elastic properties of tissues *Proc. Inst. Mech. Eng.* H **213** 203–33

Papazoglou S, Hamhaber U, Braun J and Sack I 2008 Algebraic Helmholtz inversion in planar magnetic resonance elastography *Phys. Med. Biol.* **53** 3147–58

Papazoglou S, Hirsch S, Braun J and Sack I 2012 Multifrequency inversion in magnetic resonance elastography *Phys. Med. Biol.* **57** 2329–46

Parker K J, Doyley M M and Rubens D J 2011 Imaging the elastic properties of tissue: the 20 year perspective *Phys. Med. Biol.* **56** R1–29

Patel A P *et al* 2014 Single-cell RNA-seq highlights intratumoral heterogeneity in primary glioblastoma *Science* **344** 1396–401

Perrinez P R, Kennedy F E, Van Houten E E W, Weaver J B and Paulsen K D 2010 Magnetic resonance poroelastography: an algorithm for estimating the mechanical properties of fluid-saturated soft tissues *IEEE Trans. Med. Imaging* **29** 746–55

Posnansky O, Guo J, Hirsch S, Papazoglou S, Braun J and Sack I 2012 Fractal network dimension and viscoelastic powerlaw behavior: I. A modeling approach based on a coarse-graining procedure combined with shear oscillatory rheometry *Phys. Med. Biol.* **57** 4023–40

Reiss-Zimmermann M, Streitberger K-J, Sack I, Braun J, Arlt F, Fritzsch D and Hoffmann K T 2014 High resolution imaging of viscoelastic properties of intracranial tumours by multi-frequency magnetic resonance elastography *Clin. Neuroradiol.* **25** 371–80

Riek K, Millward J M, Hamann I, Mueller S, Pfueller C F, Paul F, Braun J, Infante-Duarte C and Sack I 2012 Magnetic resonance elastography reveals altered brain viscoelasticity in experimental autoimmune encephalomyelitis *NeuroImage: Clin.* **1** 81–90

Romano A, Guo J, Prokscha T, Meyer T, Hirsch S, Braun J, Sack I and Scheel M 2014 *In vivo* waveguide elastography: effects of neurodegeneration in patients with amyotrophic lateral sclerosis *Magn. Reson. Med.* **72** 1755–61

Romano A, Scheel M, Hirsch S, Braun J and Sack I 2012 *In vivo* waveguide elastography of white matter tracts in the human brain *Magn. Reson. Med.* **68** 1410–22

Rustogi R, Horowitz J, Harmath C, Wang Y, Chalian H, Ganger D R, Chen Z E, Bolster B D, Shah S and Miller F H 2012 Accuracy of MR elastography and anatomic MR imaging features in the diagnosis of severe hepatic fibrosis and cirrhosis *J. Magn. Reson. Imaging* **35** 1356–64

Sack I, Beierbach B, Hamhaber U, Klatt D and Braun J 2008 Non-invasive measurement of brain viscoelasticity using magnetic resonance elastography *NMR Biomed.* **21** 265–71

Sack I, Beierbach B, Wuerfel J, Klatt D, Hamhaber U, Papazoglou S, Martus P and Braun J 2009 The impact of aging and gender on brain viscoelasticity *NeuroImage* **46** 652–7

Sack I, Johrens K, Wurfel J and Braun J 2013 Structure-sensitive elastography: on the viscoelastic powerlaw behavior of *in vivo* human tissue in health and disease *Soft Matter* **9** 5672–80

Sack I, Streitberger K J, Krefting D, Paul F and Braun J 2011 The influence of physiological aging and atrophy on brain viscoelastic properties in humans *PLoS One* **6** e23451

Schiessel H, Metzler R, Blumen A and Nonnenmacher T F 1995 Generalized viscoelastic models: their fractional equations with solutions *J. Phys. A: Math. Gen.* **28** 6567

Schofield M A and Zhu Y 2003 Fast phase unwrapping algorithm for interferometric applications *Opt. Lett.* **28** 1194–6

Schregel K, Wuerfel née Tysiak E, Garteiser P, Gemeinhardt I, Prozorovski T, Aktas O, Merz H, Petersen D, Wuerfel J and Sinkus R 2012 Demyelination reduces brain parenchymal stiffness quantified *in vivo* by magnetic resonance elastography *Proc. Natl. Acad. Sci. USA* **109** 6650–5

Schulz-Schaeffer W J 2010 The synaptic pathology of alpha-synuclein aggregation in dementia with Lewy bodies, Parkinson's disease and Parkinson's disease dementia *Acta. Neuropathol.* **120** 131–43

Schwarb H, Johnson C L, McGarry M D J and Cohen N J 2016 Medial temporal lobe viscoelasticity and relational memory performance *NeuroImage* **132** 534–41

Seelaar H, Rohrer J D, Pijnenburg Y A L, Fox N C and van Swieten J C 2011 Clinical, genetic and pathological heterogeneity of frontotemporal dementia: a review *J. Neurol. Neurosurg. Psychiatry* **82** 476–86

Siegmann K C, Xydeas T, Sinkus R, Kraemer B, Vogel U and Claussen C D 2010 Diagnostic value of MR elastography in addition to contrast-enhanced MR imaging of the breast-initial clinical results *Eur. Radiol.* **20** 318–25

Simon M, Guo J, Papazoglou S, Scholand-Engler H, Erdmann C, Melchert U, Bonsanto M, Braun J, Petersen D, Sack I and Wuerfel J 2013 Non-invasive characterization of intracranial tumors by magnetic resonance elastography *New J. Phys.* **15** 085024

Sinkus R, Daire J L, Beers B V and Vilgrain V 2010 Elasticity reconstruction: Beyond the assumption of local homogeneity *C. R. Mec.* **338** 474–9

Sinkus R, Lorenzen J, Schrader D, Lorenzen M, Dargatz M and Holz D 2000 High-resolution tensor MR elastography for breast tumour detection *Phys. Med. Biol.* **45** 1649–64

Sinkus R, Siegmann K, Xydeas T, Tanter M, Claussen C and Fink M 2007 MR elastography of breast lesions: understanding the solid/liquid duality can improve the specificity of contrast-enhanced MR mammography *Magn. Reson. Med.* **58** 1135–44

Sinkus R, Tanter M, Xydeas T, Catheline S, Bercoff J and Fink M 2005 Viscoelastic shear properties of *in vivo* breast lesions measured by MR elastography *Magn. Reson. Imaging* **23** 159–65

Streitberger K J, Guo J, Tzschätzsch H, Hirsch S, Fischer T, Braun J and Sack I 2014a High-resolution mechanical imaging of the kidney *J. Biomech.* **47** 639–44

Streitberger K J, Reiss-Zimmermann M, Freimann F B, Bayerl S, Guo J, Arlt F, Wuerfel J, Braun J, Hoffmann K-T and Sack I 2014b High-resolution mechanical imaging of glioblastoma by multifrequency magnetic resonance elastography *PLoS One* **9** e110588

Streitberger K-J, Sack I, Krefting D, Pfuller C, Braun J, Paul F and Wuerfel J 2012 Brain viscoelasticity alteration in chronic-progressive multiple sclerosis *PLoS One* **7** e29888

Streitberger K-J *et al* 2010 *In vivo* viscoelastic properties of the brain in normal pressure hydrocephalus *NMR. Biomed.* **24** 385–92

Su Y, Ma J, Du L, Xia J, Wu Y, Jia X, Cai Y, Li Y, Zhao J and Liu Q 2015 Evaluation of neonatal brain development using acoustic radiation force impulse imaging (ARFI) *J. Neurophysiol.* **47** 322–5

Szabo T L and Wu J 2000 A model for longitudinal and shear wave propagation in viscoelastic media *J. Acoust. Soc. Am.* **107** 2437–46

Urayama K, Kawamura T and Kohjiya S 2009 Structure-mechanical property correlations of model siloxane elastomers with controlled network topology *Polymer* **50** 347–56

Van Houten E E W 2014 Parameter identification in a generalized time-harmonic Rayleigh damping model for elastography *PLoS One* **9** e93080

Van Houten E E W, Paulsen K D, Miga M I, Kennedy F E and Weaver J B 1999 An overlapping subzone technique for MR-based elastic property reconstruction *Magn. Reson. Med.* **42** 779–86

Van Houten E E W, Viviers D R, McGarry M D J, Perrinez P R, Perreard I I, Weaver J B and Paulsen K D 2011 Subzone based magnetic resonance elastography using a Rayleigh damped material model *Med. Phys.* **38** 1993–2004

Venkatesh S K, Yin M and Ehman R L 2013 Magnetic resonance rlastography of liver: technique, analysis, and clinical applications *J. Magn. Reson. Imaging* **37** 544–55

Weaver J B, Pattison A J, McGarry M D, Perreard I M, Swienckowski J G, Eskey C J, Lollis S S and Paulsen K D 2012 Brain mechanical property measurement using MRE with intrinsic activation *Phys. Med. Biol.* **57** 7275–87

Wuerfel J, Paul F, Beierbach B, Hamhaber U, Klatt D, Papazoglou S, Zipp F, Martus P, Braun J and Sack I 2010 MR-elastography reveals degradation of tissue integrity in multiple sclerosis *NeuroImage* **49** 2520–5

Xu L, Lin Y, Han J C, Xi Z N, Shen H and Gao P Y 2007a Magnetic resonance elastography of brain tumors: preliminary results *Acta. Radiol.* **48** 327–30

Xu L, Lin Y, Xi Z N, Shen H and Gao P Y 2007b Magnetic resonance elastography of the human brain: a preliminary study *Acta. Radiol.* **48** 112–5

Zhang J, Green M A, Sinkus R and Bilston L E 2011 Viscoelastic properties of human cerebellum using magnetic resonance elastography *J. Biomech.* **44** 1909–13